

Original Article

Cite this article: Shirmohammadi M, Sepahi AA, Santos JF, Maanijou M, Torkian A, and Vahidpour H (2023) Geochemistry and Sr–Nd isotopic characteristics of ferroan–magnesian metaluminous granites of the NW Sanandaj–Sirjan zone, Iran: granite formation in a compressional–extensional setting during Late Jurassic time. *Geological Magazine* **160**: 1065–1089. <https://doi.org/10.1017/S0016756823000146>

Received: 8 February 2022

Revised: 22 February 2023

Accepted: 23 February 2023

First published online: 3 April 2023

Keywords:


A-type granites; Almogholagh–Dehgolan; ferroan; weakly extensional regime; Sanandaj–Sirjan zone

Author for correspondence:

Ali A. Sepahi,
Emails: aasepahi@gmail.com,
sepahi@basu.ac.ir

*Present address: Department of Geology, Faculty of Science, Ferdowsi University of Mashhad, Iran

Geochemistry and Sr–Nd isotopic characteristics of ferroan–magnesian metaluminous granites of the NW Sanandaj–Sirjan zone, Iran: granite formation in a compressional–extensional setting during Late Jurassic time

Majid Shirmohammadi¹, Ali Asghar Sepahi^{1,*} , José Francisco Santos² ,
Mohammad Maanijou¹, Ashraf Torkian¹ and Hamed Vahidpour¹

¹Department of Geology, Bu-Ali Sina University, Hamedan, Iran and ²Department of Geosciences, Geobiotec Research Unit, Aveiro University, Aveiro, Portugal

Abstract

The Almogholagh–Dehgolan region is in the North Sanandaj–Sirjan zone of NW Iran. The granites of the region are metaluminous and display geochemical and textural characteristics of transitional granites between ferroan (A-type) and I-type granites. In geotectonic discrimination diagrams, the Almogholagh–Dehgolan granites plot mainly in the fields of within-plate granites and volcanic arc granites. With the exception of the Qalaylan granites, parts of other granites resemble A₂-type granites. Granites of the Qalaylan intrusive body have petrographic and geochemical features close to I-type granites and are not A-type. Primary mantle and chondrite-normalized spider diagrams show enrichments in light rare earth elements relative to heavy rare earth elements. For an age of 150 Ma, the initial ⁸⁷Sr/⁸⁶Sr and ¹⁴³Nd/¹⁴⁴Nd ratios vary from 0.702769 to 0.706545 and from 0.512431 to 0.512558, respectively. Epsilon Nd values vary in a relatively limited range between –0.3 and +2.2, which corresponds to a mixed mantle–crustal source. On the basis of new geochemical and isotopic data, we suggest a geodynamic model involving partial melting of lower crustal rocks with the contribution of mantle magmas in a weakly extensional tectonic setting for the generation of the A-type granites of the region. The occurrence of ferroan (A-type) granites in this region of the Sanandaj–Sirjan zone indicates the existence of a partly extensional tectonic environment in a mainly compressional subduction-related regime in Late Jurassic time.

1. Introduction

Granitoids are the most abundant igneous rocks in the Earth's upper continental crust and like other igneous rocks represent information about internal parts of the Earth. Petrogenesis of these rocks is closely connected with tectonics and geodynamics. As defined by Loiselle & Wones (1979), A-type granitoids are referred to as a group of rocks that form in anorogenic tectonic settings. The origin of A-type granites is generally connected with an extensional regime in the lithosphere (Bonin, 2007). The occurrence of A-type granites can also indicate collided plate suture zones (Balen *et al.* 2020). A-type granites are geochemically characterized by elevated high-field-strength elements (HFSEs) (Zr, Nb, Ta), rare earth elements (REEs) (except Eu) and F contents, and high FeO_t/MgO and Ga/Al ratios and low CaO and trace elements such as Co, Sc, Cr, Ni, Ba, Sr and Eu (Loiselle & Wones, 1979; Collins *et al.* 1982; Whalen *et al.* 1987; Eby, 1990; Bonin, 2007; Whalen & Hildebrand, 2019; Bonin *et al.* 2020). Eby (1992) subdivided A-type granites into two main types, A₁ and A₂. The A₂-type granites form in post-collisional and/or post-orogenic tectonic settings and they occur in a short time interval (10–20 Myr) after compressional tectonics (Eby, 2011). The source and formation mechanisms of A-type granites are controversial, and different sources from mantle to crustal or mixed-sources (mantle–crustal) have been considered for their generation (Eby, 1990; Bonin, 2007; Shellnutt & Zhou, 2007; Frost & Frost, 2011; Grebennikov, 2014; Lu *et al.* 2020). Frost & Frost (2011) suggested that it could be better if the A-type idiom was replaced by ferroan, but because of the wide usage of the A-type idiom before and after their suggestion, we prefer not to abandon this term completely. Regardless of the source type, the generating mechanisms of these rocks can be summarized into three main categories: partial melting, fractional crystallization, and magma mixing or hybridization.

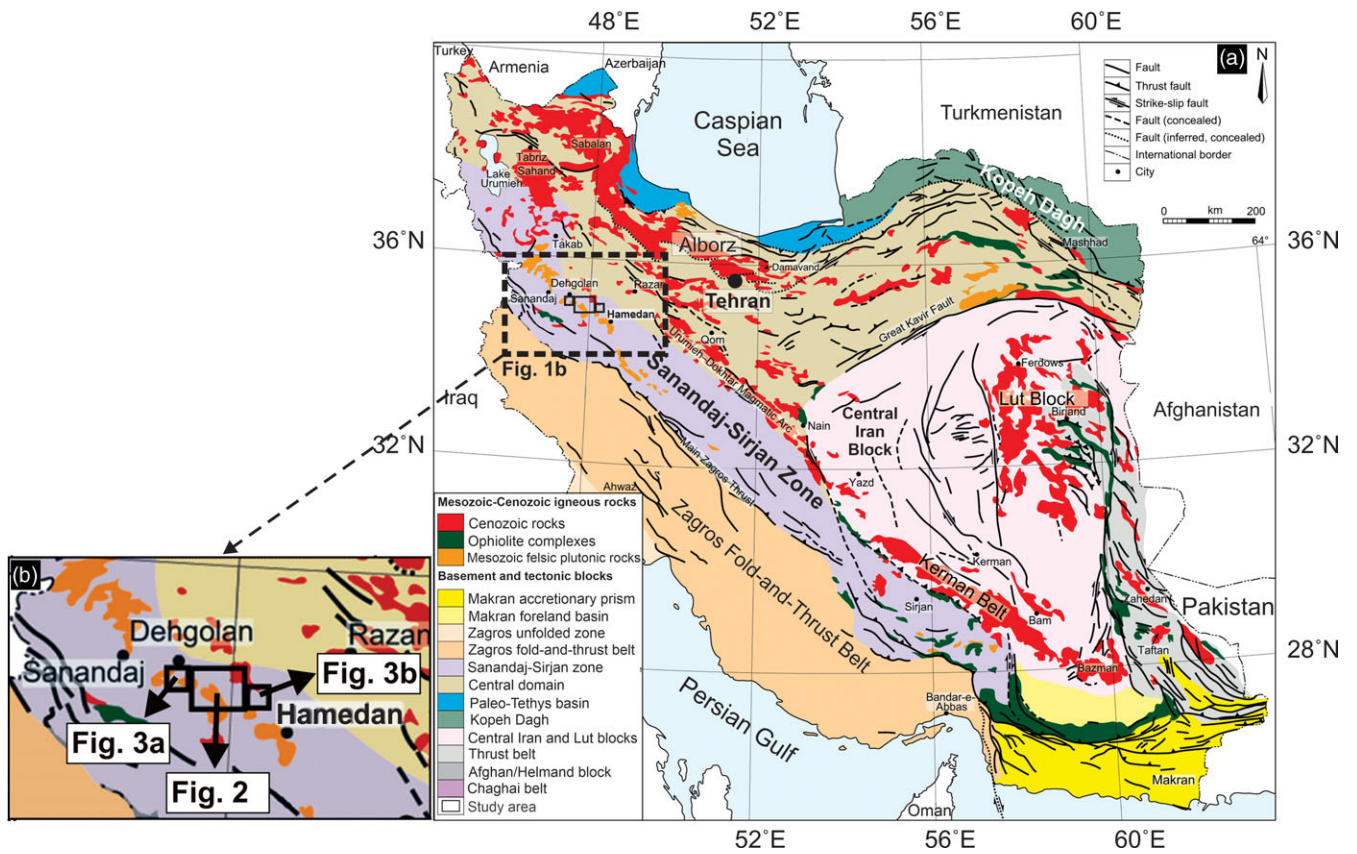


Fig. 1. (Colour online) (a) Simplified geological map and tectonic subdivisions of the Iranian Plateau (modified after Richards *et al.* 2012). (b) The general location of the Almogholagh-Dehghan region in the NSaSZ.

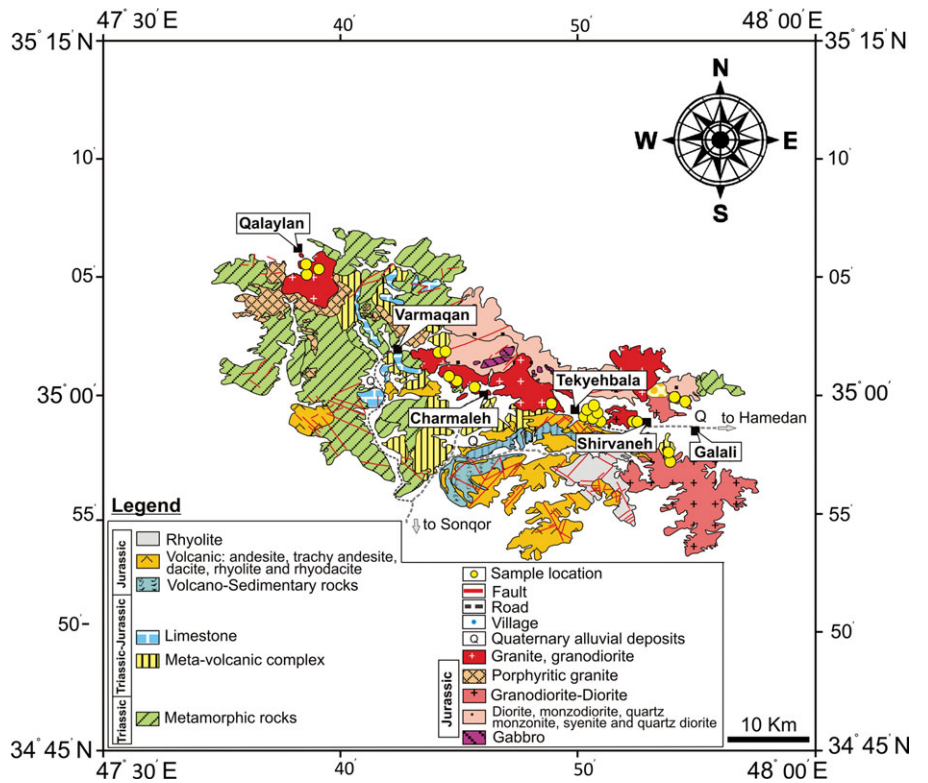


Fig. 2. (Colour online) Geological map of the area including the Galali, Shirvaneh, Tekyehbala, Charmaleh, Varmaqan and Qalaylan intrusive bodies (modified after Hosseini *et al.* 1999).

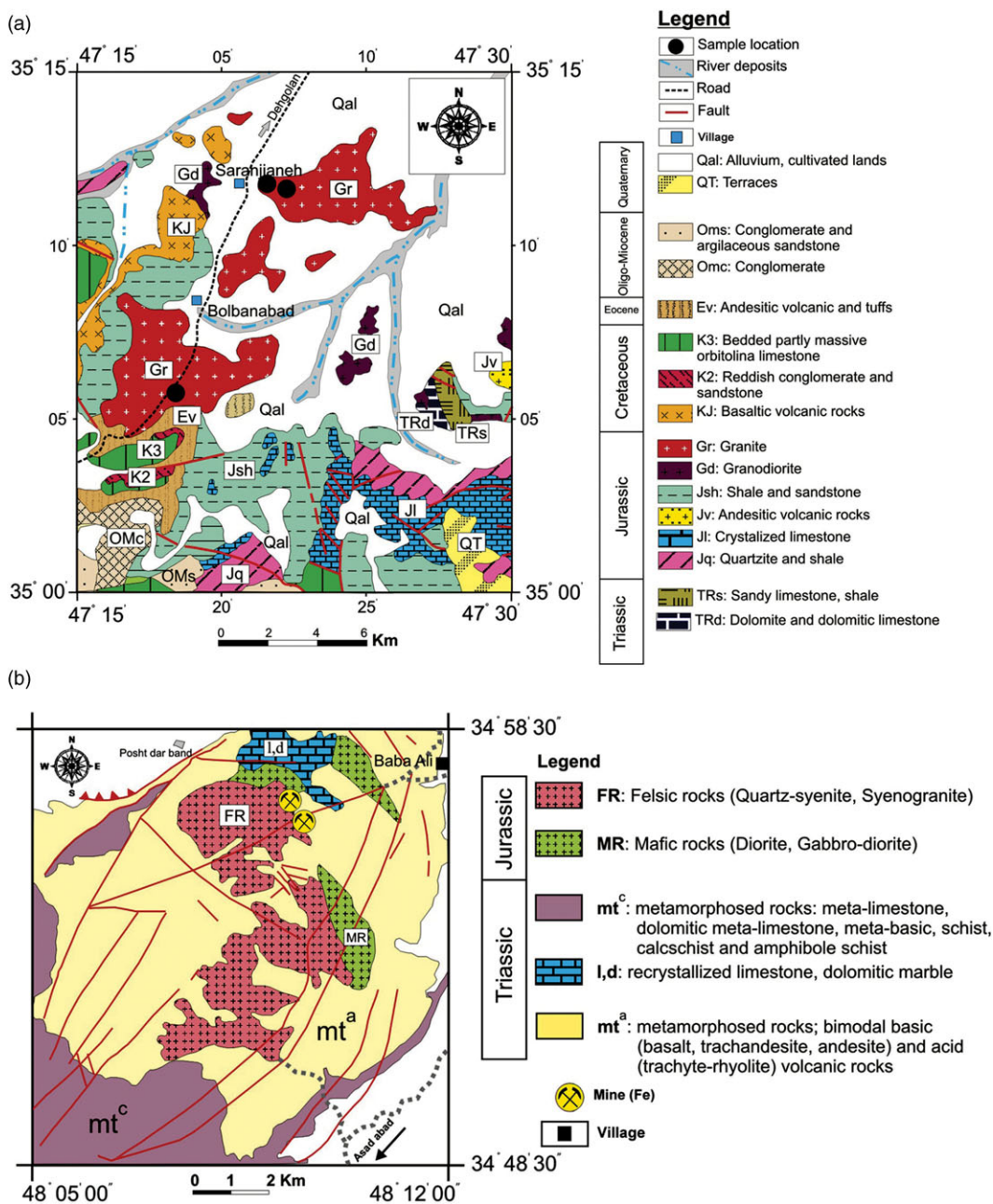


Fig. 3. (Colour online) (a) Geological map of the Saranjaneh-Bolbanabad intrusive bodies (modified after Zahedi & Hajian, 1985). (b) Geological map of the Almogholagh region (modified after Eshraghi & Mahmoudi Gharai, 2003).

The Iranian Plateau, as a part of Alpine–Himalayan orogenic belt, has an important geological situation. The geology and tectonic style of Iran are highly influenced by the history and evolution of the Tethyan oceans (Mehdipour Ghazi & Moazzen, 2015). As illustrated in Figure 1a, the Iranian Plateau has been divided into several structural zones, namely the Zagros, Makran, Sanandaj–Sirjan zone, Urmia–Dokhtar magmatic assemblage, Central Iran block, Alborz magmatic zone, Sistan Suture zone and other zones. The simplified geological map of Iran is shown in Figure 1a. The Sanandaj–Sirjan zone (SaSZ) is a narrow metamorphic and magmatic band that extends c. 1500 km from northwest (Sanandaj) to southeast (Sirjan) with a width of 150–200 km and is parallel to the Zagros Fold-Thrust belt (Mohajjel & Fergusson, 2000; Esna-Ashari *et al.* 2012; Mehdipour Ghazi & Moazzen, 2015). The SaSZ is the highly deformed part of the Zagros Orogen and has a NW–SE structural trend.

The geological history and tectonic setting of the SaSZ are controversial, and different models including continental magmatic arc (e.g. Arvin *et al.* 2007; Torkian *et al.* 2008; Maanijou *et al.* 2013; Moinevaziri *et al.* 2015; Hassanzadeh & Wernicke, 2016; Sepahi *et al.* 2018; Elahi-Janatmakan *et al.* 2020; Moradi *et al.* 2020; Shakerardakani *et al.* 2020; Maghdour-Mashhour *et al.* 2021) and/or even continental rift tectonic settings (Hunziker *et al.* 2015; Azizi *et al.* 2018; Azizi & Stern, 2019; Azizi, 2020) have been suggested for this zone.

Using the geochemical evidence, some researchers have promoted the propagation of a continental rift in the entire SaSZ during Jurassic time (Hunziker *et al.* 2015; Lechmann *et al.* 2018; Azizi & Stern, 2019; Azizi, 2020) and that the initiation of subduction occurred during mid-Cretaceous time (Shafaii Moghadam *et al.* 2020). However, a continental rift model for the SaSZ is at odds with many observations and geochemical data (voluminous

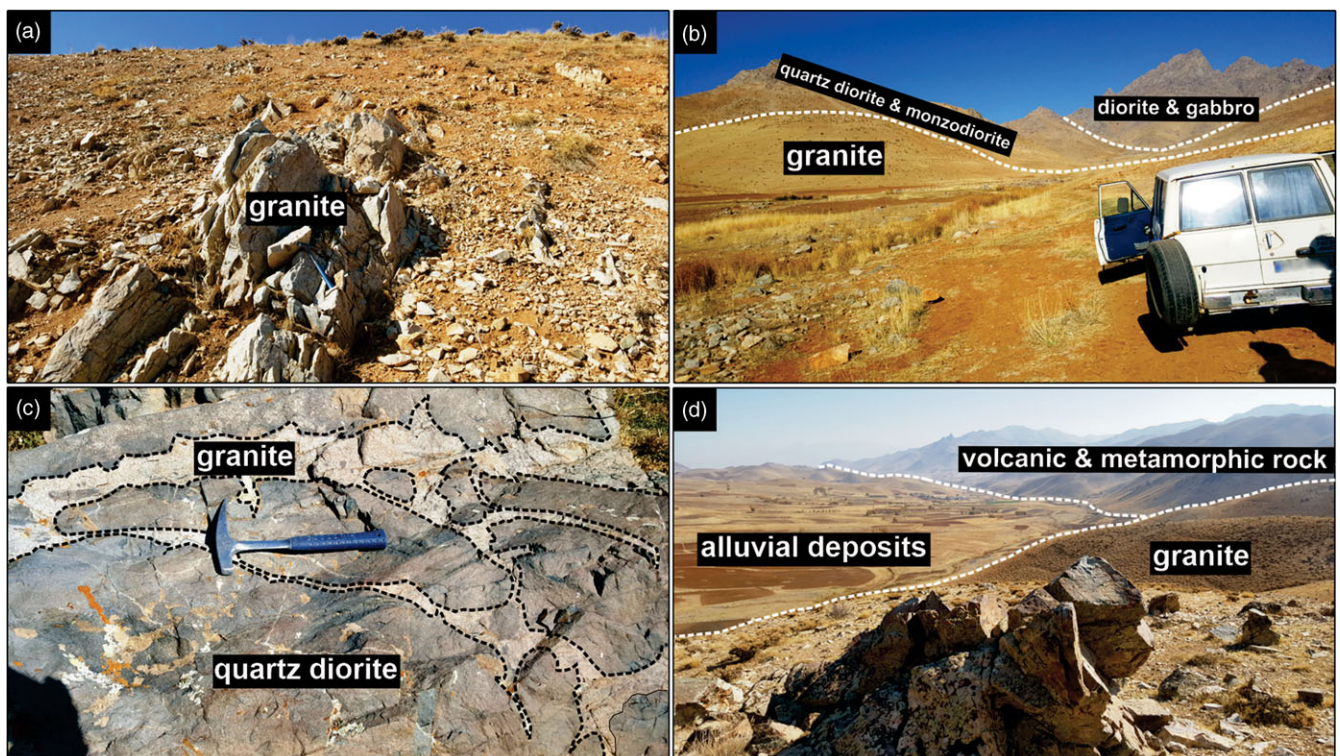


Fig. 4. (Colour online) Photographs showing a general view and field relationships of the granitic rocks (Almogholagh–Dehgolan region). (a) There are different rock suites around Tekyehbala village as a part of the Almogholagh–Dehgolan region (view direction is towards the southeast). (b) The granites of the area have a sharp contact with the host dioritic and mafic rocks (view direction is towards the northwest). (c) Irregular and vein granitic dykes (light grey) penetrated as a network into the host dioritic rocks (dark grey). This picture may also show evidence of coeval intrusion of mafic and felsic magmas. (d) An outcrop showing the granites of the area, which are white-light grey and medium to fine grained. Hammer for scale is ~35 cm long.

calc-alkaline arc rocks of Jurassic age) that have previously been reported (Elahi-Janatmakan *et al.* 2020; Maghdour-Mashhour *et al.* 2021). Moreover, there is no stratigraphic record showing mid-Jurassic continental rifting in the central SaSZ (Elahi-Janatmakan *et al.* 2020).

During Palaeozoic time, the SaSZ was a part of NE Gondwana and was separated from the Eurasian plate by the Palaeo-Tethys Ocean. The initiation of northward subduction of the Neo-Tethys beneath the Iranian Plateau occurred during Late Triassic – Early Jurassic time (Agard *et al.* 2011; Hassanzadeh & Wernicke, 2016; Elahi-Janatmakan *et al.* 2020). Early to Middle Jurassic arc magmatism is considered to record a period of subduction of the Neo-Tethys oceanic plate, as reflected in voluminous calc-alkaline, metaluminous I-type granites and mafic magmatism (Shakerardakani *et al.* 2020). In all sectors of the SaSZ, the dominance of calc-alkaline rocks that are largely subparallel to the Zagros suture is robust evidence for their formation in a continental arc setting (Maghdour-Mashhour *et al.* 2021). The arc magmatism was followed by emplacement of Late Jurassic to Early Cretaceous A- and S-type granites into Jurassic metamorphic host rocks through the SaSZ (Fazlnia *et al.* 2009; Azizi & Asahara, 2013; Azizi *et al.* 2016; Yang *et al.* 2018). Collision of the Arabian and Eurasian continents occurred during Late Cretaceous to Oligocene time (McQuarrie *et al.* 2003) and caused the formation of the Urumieh–Dokhtar magmatic arc (Verdel *et al.* 2011). However, the timing of the Arabia–Eurasia collision along the Main Zagros Thrust is controversial, and a time between 35 and 5 Ma has been suggested for it (Omran *et al.* 2008; Agard *et al.* 2011; Cowgill *et al.* 2016; Zhang, Z. *et al.* 2018).

Most Jurassic granitoids of the SaSZ mainly have I-type characteristics and are related to active continental margin magmatism (arc-type magma) in a subduction environment due to subduction of the Neo-Tethys oceanic crust beneath the Central Iranian Microplate (Ahmadi Khalaji *et al.* 2007; Torkian *et al.* 2008; Mahmoudi *et al.* 2011; Jamshidibadr *et al.* 2018; Tavakoli *et al.* 2021). In addition to I-type granites, A-type granites have also been reported from some localities of the SaSZ (e.g. Sepahi & Athari, 2006; Mansouri Esfahani *et al.* 2010; Alirezai & Hassanzadeh, 2012; Maanijou *et al.* 2013; Sarjoughian *et al.* 2015; Shahbazi *et al.* 2015; Yajam *et al.* 2015; Tavakoli *et al.* 2021). In the studied area, there are several granitoid bodies that are scattered from the Almogholagh region in the southeast to the Dehgolan region in the northwest. From a petrological point of view, the spatial and temporal co-development of A- and I-type granites in the North Sanandaj–Sirjan Zone (NSaSZ) is very important. As suggested by Eby (1992), A-type granites, as good indicators of tectonic settings, may provide significant constraints on the origin of magmatism. The close association of A- and I-type granites provides a great opportunity to examine their origins and relationships. If the granites of the studied area are considered, there are several questions, including: (1) What are the field, petrographic, geochemical and isotopic characteristics of A-type granites compared to I-type granites in the Almogholagh–Dehgolan region, as a part of the NSaSZ? (2) Is there a genetic relationship between A- and I-type granites in the area? (3) What was the cause of the A-type magmatism in the region? (4) What was the tectonic setting in which the studied granites were formed? (5) How is the association of A- and I-type granites in the studied area explained? These and

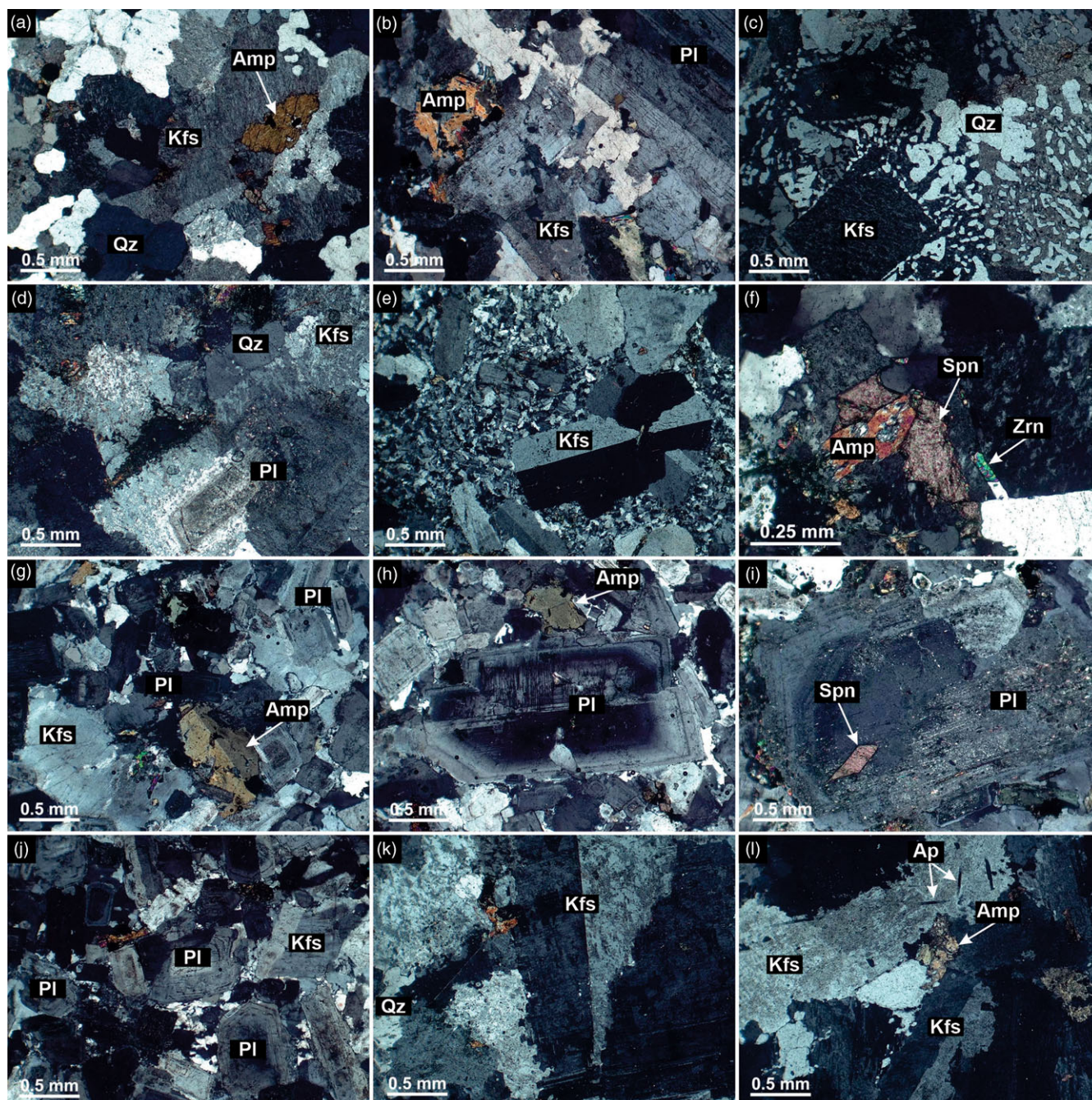


Fig. 5. (Colour online) Photomicrographs displaying the main constituent minerals of the Almogholagh–Dehgolan granitic rocks and their petrographic features (cross-polarized light). (a) The main constituent minerals of the Almogholagh–Dehgolan granitic rocks, including quartz, K-feldspar and plagioclase. (b) Perthitic orthoclase with Carlsbad twinning in the studied granites. (c) In the granites, plagioclase shows compositional zoning and is altered to sericite and epidote. (d) Mafic minerals including amphibole and biotite are common in the granites. (e) Secondary minerals including epidote, chlorite and sericite. (f) Photomicrograph showing the accessory minerals including sphene and Fe–Ti oxides in the Almogholagh–Dehgolan granites. (g) Granophyric texture is the most common intergrowth texture of the granites. (h) Photomicrograph showing anti-rapakivi texture in the granites, in which plagioclase is rimmed by overgrown K-feldspar. (i) Mylonitic texture/structure in the granites. Coarse twinned K-feldspar crystals have been formed in the fine groundmass comprising quartz, K-feldspar and plagioclase. Similar mineral assemblages are seen in the granites of the plutons. Abbreviations are after Whitney & Evans (2010).

some more questions are the main scientific problems that will be argued in the present research.

2. Geological setting

Several igneous plutons with different sizes and mafic to intermediate and felsic compositions have been exposed. From the

southeast to the northwest, intrusive bodies include the Almogholagh, Galali, Shirvaneh, Tekyehbala, Charmaleh, Varmaqan, Qalaylan, Saranjaneh and Bolbanabad. These stocks and plutons have all been emplaced into Jurassic metamorphic units and have various compositions that range from gabbro to granite. The granitoid intrusive bodies are generally called the Almogholagh–Dehgolan granitoids. The general location of the

Table 1. Calculated approximate percentage of modal felsic minerals (QAP) for the Almoghlagh–Dehgalan granites

Sample ID	Q	A	P	Sum	Rock name
AM20m	30	45	25	100	Granite
AM21m	35	40	25	100	Granite
AM22m	40	40	20	100	Granite
GL77	40	30	30	100	Granite
GL79	35	30	35	100	Granite
GL21m	15	75	10	100	Quartz syenite
GL22m	30	40	30	100	Granite
SH63	30	45	25	100	Granite
SH65	35	40	25	100	Granite
TK15-1	40	45	15	100	Granite
TK33	30	45	25	100	Granite
TK40	25	55	20	100	Granite
TK45	35	55	10	100	Granite
TK52	40	30	30	100	Granite
TK56	30	35	35	100	Granite
TK82	30	50	20	100	Granite
CH93-3	35	25	40	100	Granite
CH106	10	70	20	100	Quartz syenite
CH123-1	30	45	25	100	Granite
VM142	15	70	15	100	Quartz syenite
VM143	35	35	30	100	Granite
QL167	35	35	30	100	Granite
QL169	40	40	20	100	Granite
QL186	30	35	35	100	Granite
SJ02	40	30	30	100	Granite
SJ04	35	40	25	100	Granite
BA17-1	40	40	20	100	Granite

Abbreviations: Q – quartz; A – alkali-feldspar; P – plagioclase.

area is shown in Figure 1b. The geological map of the Galali, Shirvaneh, Tekyehbala, Charmaleh, Varmaqan and Qalaylan plutons is illustrated in Figure 2. Figure 3a, b shows the geological map of the Saranjianeh–Bolbanabad and Almoghlagh intrusive bodies. Towards the Hamedan region, these plutons (a) intruded Middle Jurassic regional metamorphic rocks known as the ‘Hamedan Phyllites’ (Monfaredi *et al.* 2016), (b) intruded an Upper Jurassic pyroclastic sequence towards the Sonqor region, and (c) finally were emplaced in an Upper Triassic to Jurassic metabasite sequence in the Qorveh region (Eshraghi *et al.* 1996; Hosseini *et al.* 1999). Generally, metamorphic rocks occur in a vast portion of the area and are composed of schist, marble, amphibolite and gneiss that together with the igneous plutonic bodies form the rough topography of the region. The plutonic igneous bodies are gabbro-diorite, diorite, granodiorite, syenite and granite, which are younger in age than the metamorphic rocks. Volcano-sedimentary rocks include rhyolitic to rhyodacitic tuffs with trachyandesite of Jurassic–Cretaceous age.

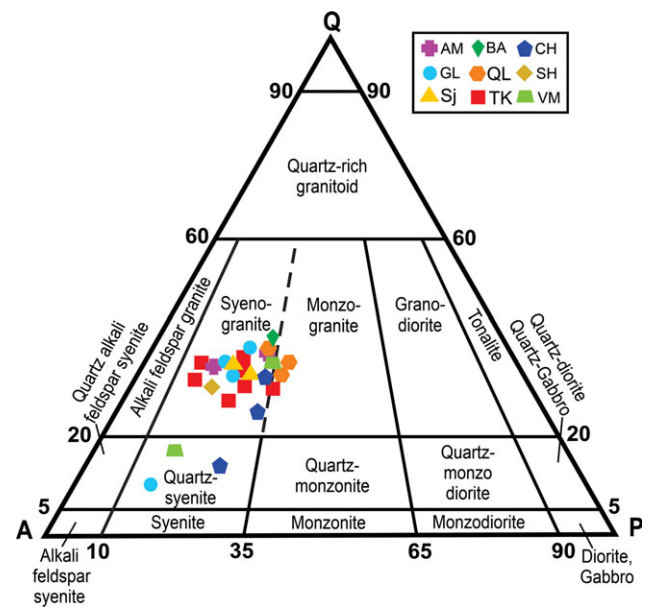


Fig. 6. (Colour online) Modal QAP classification diagram of plutonic rocks (Streckeisen, 1979) for the Almoghlagh–Dehgalan granitic rocks. AM – Almoghlagh; GL – Galali; SH – Shirvaneh; TK – Tekyehbala; CH – Charmaleh; VM – Varmaqan; QL – Qalaylan; SJ – Saranjianeh; BA – Bolbanabad.

The I-type granites of the NSaSZ mainly have the geochemical characteristics of arc-related magmas (e.g. Sepahi & Athari, 2006; Ahmadi Khalaji *et al.* 2007; Torkian *et al.* 2008; Mahmoudi *et al.* 2011; Maanjou *et al.* 2013; Sarjoughian *et al.* 2015; Yajam *et al.* 2015; Amiri *et al.* 2017; Jamshidibadr *et al.* 2018). In the case of the Qalaylan granitoids, Azizi *et al.* (2015) suggested that these rocks are geochemically similar to high-silica adakites and Archaean tonalite–trondhjemite–granodiorite (TTG) rocks and that their generation was related to an extensional basin, such as a back-arc setting, which had been developed between the Sonqor–Qorveh island arc and the SaSZ. As suggested by Yajam *et al.* (2015), subduction-related magmatism started in Early Jurassic time and included the southern plutonic bodies of the NSaSZ and continued to the Galali pluton with the formation of a mafic-rock source magma during Late Jurassic time (~160 Ma). Zhang, H. *et al.* (2018) geochemically subdivided the plutonic rocks of the Qorveh Plutonic Complex (QPC) into two groups. They proposed that the Mobarak Abad diorites and Qorveh gabbros and diorites most likely formed from magmas derived from a subduction-modified region of the subcontinental lithospheric mantle. In comparison, the Qorveh A-type quartz monzonites formed from a quartzo-feldspathic igneous crustal source, whereas the Bolbanabad A-type granites were probably formed from depleted mantle-derived magmas that underwent assimilation and fractional crystallization processes. They suggested a slab window geodynamic model for the generation of the QPC during subduction of the Neo-Tethys. Yeganeh *et al.* (2018) also pointed to an intra-arc extensional tectonic setting for the generation of the mafic to intermediate rocks of the Darvazeh plutonic suite (south Qorveh) in Late Jurassic time, and suggested that these rocks were formed in a continental arc experiencing extension as the Neo-Tethys oceanic lithosphere subducted beneath the Central Iranian Plate. Recently, Azizi *et al.* (2020) suggested that the mafic–intermediate and felsic rocks in southern Qorveh (Meiham–Shirvaneh) were formed in an

Table 2. CIPW normative minerals for the studied samples

Sample ID	Qz	Crn	Or	Ab	An	Di	Hyp	Mag	Ilm	Ap
AM20	29.73	0.64	11.23	42.05	11.64	–	3.49	0.14	0.68	0.02
AM21	19.32	–	31.97	35.29	5.22	1.21	4.07	0.20	0.68	0.12
AM22	23.35	–	33.33	32.15	5.14	1.68	2.74	0.16	0.65	0.09
GL77	10.11	–	20.51	51.19	6.20	1.76	9.16	0.43	1.44	0.30
GL79	14.52	–	1.30	68.03	6.15	7.41	–	0.10	1.67	0.42
GL21m	2.93	–	22.34	40.36	10.07	18.69	0.13	0.29	3.27	1.04
GL22m	17.51	–	31.50	41.89	4.44	1.90	0.42	0.09	1.04	0.19
SH63	21.49	–	29.55	37.74	5.35	1.40	3.58	0.19	0.76	0.12
SH65	21.97	–	33.33	34.78	4.05	0.81	4.51	0.22	0.70	0.12
TK15	14.68	–	27.89	38.67	7.40	7.29	2.05	0.22	1.46	0.37
TK33	22.35	–	30.02	35.71	5.92	2.88	1.91	0.14	1.04	0.16
TK40	24.69	–	27.78	35.96	5.21	2.17	1.41	0.12	0.93	0.16
TK45	22.08	–	30.08	36.81	5.31	3.04	1.15	0.14	1.04	0.19
TK52	29.17	–	7.21	49.84	10.67	0.38	–	0.04	1.06	0.02
TK56	23.55	0.25	0.35	69.89	2.49	–	2.79	0.12	0.91	0.14
TK82	12.51	–	5.26	62.62	5.33	5.37	5.17	0.32	1.56	0.37
CH93	15.01	–	18.97	56.27	4.22	4.77	–	0.10	1.35	0.25
CH106	5.63	–	4.73	65.66	7.25	13.09	–	0.26	2.75	0.81
CH123	18.99	–	4.43	56.95	10.66	2.54	1.82	0.13	1.29	0.32
VM142	9.57	–	27.89	37.49	11.61	9.62	–	0.17	2.20	0.72
VM143	16.40	–	26.06	32.66	11.75	4.92	6.03	0.29	1.94	0.44
QL167	18.27	–	18.79	43.32	13.06	0.44	5.14	0.22	0.63	0.19
QL169	16.12	0.21	18.26	45.35	12.77	–	5.70	0.23	0.68	0.19
QL186	15.68	–	18.02	46.96	14.13	0.50	4.47	0.19	0.53	0.12
SJ02	9.29	–	32.15	43.58	4.50	2.72	6.38	0.36	1.61	0.37
SJ04	22.48	–	26.48	39.35	5.49	1.32	1.66	0.10	0.85	0.14
BA17	28.25	0.30	30.61	31.48	2.80	–	3.33	0.16	0.32	0.05

Abbreviations: Qz – quartz; Crn – corundum; Or – orthoclase; Ab – albite; An – anorthite; Di – diopside; Hyp – hypersthene; Mag – magnetite; Ilm – ilmenite; Ap – apatite.

extensional environment (continental rift) during Late Jurassic time in the central SaSZ. However, their proposed rift model differs from the active continental margin setting of the SaSZ.

On the basis of SHRIMP U–Pb zircon dating of the seven intrusive bodies in the Qorveh–Dehgolan region, Yajam *et al.* (2015) suggested that magmatic activity spanned 20 Myr (~160–140 Ma). They also reported ages of 149 ± 2 Ma, 148 ± 1.1 Ma and 144 ± 1 Ma for the A-type granites of the Galali, Saranjaneh and Bolbanabad plutons, respectively. Jamshidibadr *et al.* (2018) detected a Late Jurassic to Early Cretaceous (148–143 Ma) crystallization age for the felsic rocks of the Almogholagh intrusive complex through U–Pb analysis of zircons. Zhang, H. *et al.* (2018) reported an age of 146 ± 2 Ma for the Bolbanabad A-type granite and interpreted this age as the timing of crystallization of the Bolbanabad pluton. Zhang, Z. *et al.* (2018) presented new zircon dating results and Hf isotope data from 22 samples of previously dated and undated granitoids in the SaSZ. In their study, a range of gabbroic to granitic lithologies were sampled from the Meso-Cenozoic intrusive rocks along the SaSZ (figs 2, 3 in Zhang, Z. *et al.* 2018). They calculated

^{206}Pb – ^{238}U ages of 153.6 ± 2.6 Ma and 150.7 ± 2.5 Ma for the Suffi Abad and Saranjaneh plutons, respectively. Their calculated age for the Saranjaneh pluton is identical (within error) to the SHRIMP zircon U–Pb age of 148 ± 1.1 Ma reported by Yajam *et al.* (2015). Furthermore, geochemical data for the samples from these two plutons suggest a typical A-type granitic signature (Zhang, Z. *et al.* 2018). They suggested that Late Jurassic magmatism is favoured to have been formed in a continental extensional environment (probably a back-arc tectonic setting) by the involvement of lower crust partial melting.

The granites from the intrusive bodies show similar field, petrographic and geochemical features. It is noteworthy that all of the abovementioned dated granites (with the exception of the Suffi Abad) are geochemically A-type granites. On the basis that some granites of the study area have already been dated by those researchers and have field, compositional and geochemical similarities, our studied granites (Almogholagh–Dehgolan region) have relatively the same age. Therefore, we have considered an average age of 150 Ma (approximately) for the granites.

Table 3. Location (UTM and geographic coordinates) of samples selected for whole-rock chemical analysis

Sample ID	Intrusive body	UTM coordinates			Geographic coordinates		Lithology
		Zone	x (m)	y (m)	Longitude (E)	Latitude (N)	
AM20m	Almogholagh	39 S	243748.0	3869263.0	48° 11' 40.08"	34° 56' 00.61"	Granite
AM21m	Almogholagh	39 S	244221.0	3869287.0	48° 11' 58.68"	34° 56' 01.82"	Granite
AM22m	Almogholagh	39 S	244381.0	3869734.0	48° 12' 04.48"	34° 56' 16.46"	Granite
GL77	Galali	38 S	764637.8	3871920.2	47° 53' 53.07"	34° 57' 19.00"	Granite
GL79	Galali	38 S	764659.2	3872606.1	47° 53' 54.72"	34° 57' 41.22"	Granite
GL21m	Galali	38 S	765407.0	3876514.0	47° 54' 33.64"	34° 59' 47.68"	Quartz syenite
GL22m	Galali	38 S	765044.0	3876753.0	47° 54' 03.80"	34° 59' 55.63"	Granite
SH63	Shirvaneh	38 S	762270.3	3874802.2	47° 52' 23.12"	34° 58' 54.65"	Granite
SH65	Shirvaneh	38 S	762455.3	3874518.6	47° 52' 30.09"	34° 58' 45.27"	Granite
TK15-1	Tekyeh	38 S	756827.7	3875771.1	47° 48' 49.77"	34° 59' 31.10"	Granite
TK33	Tekyeh	38 S	759889.3	3874590.3	47° 50' 49.09"	34° 58' 49.99"	Granite
TK40	Tekyeh	38 S	759008.2	3874778.1	47° 50' 14.59"	34° 58' 56.90"	Granite
TK45	Tekyeh	38 S	759382.5	3874471.0	47° 50' 28.98"	34° 58' 46.60"	Granite
TK52	Tekyeh	38 S	760247.0	3874690.0	47° 51' 03.26"	34° 58' 52.87"	Granite
TK56	Tekyeh	38 S	760685.6	3874443.4	47° 51' 20.28"	34° 58' 44.49"	Granite
TK82	Tekyeh	38 S	759387.1	3875613.6	47° 50' 30.46"	34° 59' 23.62"	Granite
CH93-3	Charmaleh	38 S	751781.4	3877175.4	47° 45' 32.49"	35° 00' 21.19"	Granite
CH106	Charmaleh	38 S	750759.6	3877236.0	47° 44' 52.28"	35° 00' 24.08"	Quartz syenite
CH123-1	Charmaleh	38 S	750366.2	3877885.8	47° 44' 37.49"	35° 00' 45.48"	Granite
VM142	Varmaqan	38 S	749782.3	3879837.3	47° 44' 16.59"	35° 01' 49.29"	Quartz syenite
VM143	Varmaqan	38 S	750119.5	3880121.1	47° 44' 30.18"	35° 01' 58.20"	Granite
QL167	Qalaylan	38 S	740957.7	3885685.0	47° 38' 34.79"	35° 05' 06.61"	Granite
QL169	Qalaylan	38 S	740885.6	3886489.0	47° 38' 32.80"	35° 05' 32.78"	Granite
QL186	Qalaylan	38 S	741712.6	3886134.3	47° 39' 05.05"	35° 05' 20.56"	Granite
SJ02	Saranjianeheh	38 S	715076.0	3897587.0	47° 21' 44.82"	35° 11' 53.76"	Granite
SJ04	Saranjianeheh	38 S	715367.9	3897522.0	47° 21' 56.26"	35° 11' 51.44"	Granite
BA17-1	Bolbanabad	38 S	710126.2	3886120.3	47° 18' 18.70"	35° 05' 45.60"	Granite

3. Field relationships and petrography

In the Almogholagh–Dehgolan region, the main constituent rock suites are plutonic and metamorphic rocks. In addition to the plutonic rocks, volcanic and metasedimentary rocks also occur in the area (Fig. 4). Mafic rocks, including gabbro and diorite together with volcanic and metamorphic rocks, form the rough topography of the region, and the contacts between the granites and country rocks (mafic–intermediate and metamorphic) are very distinct and sharp (Fig. 4a, b). The granites in the region are exposed as stocks or irregular dykes that intruded into the other plutonic rock suites composed of diorite, monzodiorite, quartz-monzodiorite and monzonite. On the basis of field observations, such as irregular dykes of granites intruding into the dioritic host rocks, the granites are relatively younger than the host rocks. Nevertheless, in some parts of the area, the coeval intrusion of mafic and felsic magmas occurs with cusped contacts (Fig. 4c). The Almogholagh–Dehgolan granites are white to grey and medium to fine grained (Fig. 4d). The field properties of the granites in the plutons are largely the same, and for this reason, they cannot be classified

or categorized based on their field properties. In total, 240 samples were collected from the plutons (granitoids).

Petrographic studies show that the granitoid rocks of the region have a relatively similar mineral assemblage. This assemblage includes major minerals (quartz, K-feldspar, plagioclase) and mafic minerals (amphibole, biotite). Accessory minerals (apatite, titanite, zircon, and Fe–Ti oxides) are also common in the rocks. Figure 5 shows photomicrographs of the granitoid rocks. Despite the relatively identical mineralogical composition, the granitoid rocks of the massifs are different in terms of the abundance of modal minerals, especially the main minerals, as well as textural characteristics. Therefore, according to mineralogical and textural features, the granitoids can be categorized into at least three groups as follows.

The first group includes the massifs of Almogholagh, Galali, Tekyehbala, Charmaleh, Varmaqan and Saranjianeheh–Bolbanabad. These granitoids are mainly composed of abundant K-feldspar (25–55 vol. %) with lower contents of plagioclase (10–40 vol. %). In these rocks, quartz occurs as anhedral crystals

Table 4. Major- and trace-element whole-rock compositions of granitoid rocks from the Almogholagh–Dehgolan intrusive bodies

Sample ID	AM20	AM21	AM22	GL77	GL79	GL21m	GL22m	SH63	SH65	TK15	TK33	TK40	TK45	TK52	TK56	TK82
Rock type	GR			GR	GR	QS	GR				GR				GR	
Oxides (wt %)																
SiO ₂	72.66	69.09	71.42	66.57	69.11	59.46	69.79	71.31	71.77	67.35	71.33	71.47	71.25	72.94	74.35	66.58
TiO ₂	0.36	0.36	0.34	0.76	0.88	1.72	0.55	0.4	0.37	0.77	0.55	0.49	0.55	0.56	0.48	0.82
Al ₂ O ₃	15.14	14.63	14.24	15.98	15.72	15.63	15.54	14.71	14.35	15.34	14.61	13.99	14.61	14.92	14.81	15.09
Fe ₂ O ₃	1.85	2.59	2.03	5.36	1.33	3.66	1.09	2.4	2.76	2.63	1.81	1.43	1.72	0.6	1.37	3.94
MnO	0.02	0.05	0.04	0.11	0.01	0.09	0.02	0.02	0.03	0.03	0.03	0.02	0.02	0.01	0.01	0.01
MgO	0.36	0.32	0.26	0.81	1.09	2.28	0.16	0.34	0.32	0.98	0.46	0.34	0.27	0.03	0.5	1.02
CaO	2.36	1.4	1.48	1.83	3.65	7.24	1.45	1.47	1.07	3.46	1.97	1.66	1.89	2.29	0.58	2.56
Na ₂ O	4.97	4.17	3.8	6.05	8.04	4.77	4.95	4.46	4.11	4.57	4.22	4.25	4.35	5.89	8.26	7.4
K ₂ O	1.9	5.41	5.64	3.47	0.22	3.78	5.33	5	5.64	4.72	5.08	4.7	5.09	1.22	0.06	0.89
P ₂ O ₅	0.01	0.05	0.04	0.13	0.18	0.45	0.08	0.05	0.05	0.16	0.07	0.07	0.08	0.01	0.06	0.16
LOI	1.34	0.83	0.93	0.8	0.74	0.87	1.01	0.92	0.79	0.93	0.84	0.85	1	0.87	0.99	0.37
Trace & REEs (ppm)																
V	11	12	12	33	66	150	15	14	12	76	24	19	23	20	12	69
Sc	5.5	5.2	5.1	12.8	11.8	20.1	8	5.7	5	10.1	5.6	5.4	6.1	0.8	6.4	10.5
Cr	81	48	33	38	42	33	39	39	47	38	88	41	35	56	49	45
Co	1.7	2.4	1.8	4.9	1.3	5.8	1.1	1.5	1.7	2.6	1.6	1.4	1.6	0.6	1.9	2.4
Ni	3.6	3.2	3.2	4.4	5.1	6.8	2.9	2.8	2.9	4.3	4.4	3.8	2.9	4	2.6	4.9
Ga	23.5	22.2	22.2	24.3	21.5	23.7	21.6	20.6	20.2	20.3	19.8	20.4	20.2	20	19.5	19.6
Rb	44	154.3	144.1	75.4	6.10.00	104.8	119.8	153.6	148.4	104.9	162.7	141.1	137.2	26.9	0.9	22
Sr	365	132.6	161.7	99.8	192	312.1	112.7	108.1	92.4	245.6	145.7	158.5	182.1	254.4	49.1	214.9
Y	52.7	52.8	52.2	53.1	44.2	52.4	44.4	47.7	42.3	41	43.9	41.1	47.7	22	45.3	32.1
Sn	6	5	5	5	5	5	5	8	6	5	7	5	6	5	5	5
Zr	421	373	340	725	408	391	523	399	350	394	408	419	426	377	445	425
Nb	37.2	36.5	34.5	41.5	29.2	35.8	27.4	25.5	23.5	23.7	32.5	29.9	29.8	19.3	29.5	22.4
Cs	1.07	2.47	1.95	1	0.07	1.24	0.67	0.92	0.78	0.3	0.6	0.43	0.43	0.34	0.07	0.35
Ba	212.9	526.9	566.5	549.8	80.3	536.1	657	451.7	492.5	779.2	586	606	597.6	207.7	11.8	202.5
Hf	11.4	11.1	9.8	16.7	10.3	9.7	13.2	11.2	10	10.5	11	10.9	11.3	9.9	11.3	10.9
Ta	2.2	2.1	2.1	1.9	1.7	2.1	1.7	1.7	1.8	1.7	2	1.8	1.9	1.6	1.7	1.2
Th	19.89	19.69	21.57	16.4	17.14	15.48	23.93	23.37	24.65	13.06	22.93	25.69	24.99	9.83	16.18	14.99

(Continued)

Table 4. (Continued)

Sample ID	AM20	AM21	AM22	GL77	GL79	GL21m	GL22m	SH63	SH65	TK15	TK33	TK40	TK45	TK52	TK56	TK82
Rock type		GR		GR	GR	QS	GR				GR					GR
U	3.63	5.1	5.52	3.91	4.85	4.93	4.43	4.15	5.66	4.3	6.11	5.24	6.63	2.59	3.63	4.08
La	19.1	49.1	43.9	40.5	29	37.1	27.3	35.9	59.5	29.3	42	34.7	39.3	17	28.8	29
Ce	55.7	106.5	105.1	80.9	61.3	78.2	62.4	90.2	110.8	66.9	91.5	71.6	85.2	38.9	68.4	64.5
Pr	7.41	11.82	11.93	9.34	7.12	9.38	7.51	10.53	11.27	8.27	10.3	8.28	9.57	4.54	8.76	7.47
Nd	29.9	43.1	43.1	36.1	28.5	39.7	30.4	38.7	39.6	33.2	37.1	30.5	35.8	16.3	35.5	27.3
Sm	6.95	8.27	8.54	7.9	6.34	8.95	6.82	7.65	7.4	6.82	7.03	6.34	7.38	3.19	8.08	5.58
Eu	0.81	0.99	1.03	1.97	1.45	2.21	1.29	1	1	1.28	0.97	1.02	0.98	0.77	1.3	1.46
Gd	6.68	7.89	7.97	8.02	6.5	8.88	6.53	7.21	6.9	6.6	6.53	5.81	6.97	3.01	7.15	5.32
Tb	1.21	1.3	1.3	1.34	1.06	1.44	1.12	1.16	1.1	1.07	1.07	0.95	1.17	0.52	1.18	0.88
Dy	8.35	8.62	8.56	9.01	6.88	9.1	7.7	7.78	7.01	6.69	6.84	6.29	7.7	3.47	7.66	5.57
Ho	1.75	1.74	1.81	1.88	1.49	1.84	1.61	1.64	1.47	1.44	1.45	1.34	1.63	0.73	1.51	1.11
Er	5.53	5.62	5.59	5.89	4.53	5.47	4.79	5.03	4.53	4.52	4.65	4.21	5	2.3	4.65	3.64
Tm	0.86	0.88	0.87	0.89	0.68	0.77	0.72	0.76	0.67	0.67	0.7	0.65	0.77	0.37	0.69	0.54
Yb	5.27	5.58	5.45	5.89	4.32	4.87	4.6	4.74	4.5	4.24	4.61	4.16	4.97	2.34	4.59	3.46
Lu	0.84	0.88	0.86	0.98	0.73	0.77	0.76	0.78	0.75	0.7	0.75	0.69	0.77	0.36	0.74	0.6
ΣREE	150.36	252.29	246.01	210.61	159.9	208.68	163.55	213.08	256.5	171.7	215.5	176.54	207.21	93.8	179.01	156.43
Ga/Al*10 ⁴	2.93	2.87	2.95	2.87	2.58	2.87	2.63	2.65	2.66	2.5	2.56	2.76	2.61	2.53	2.49	2.45
Y/Nb	1.42	1.45	1.51	1.28	1.51	1.46	1.62	1.87	1.8	1.73	1.35	1.37	1.6	1.14	1.54	1.43
A/CNK	1.04	0.96	0.95	0.94	0.78	0.62	0.94	0.95	0.97	0.81	0.91	0.93	0.91	0.98	1.01	0.85
(La/Yb) _N	2.47	5.99	5.48	4.68	4.57	5.18	4.04	5.15	9	4.7	6.2	5.68	5.38	4.94	4.27	5.7
(La/Sm) _N	1.72	3.72	3.22	3.21	2.87	2.6	2.51	2.94	5.04	2.69	3.74	3.43	3.34	3.24	2.23	3.26
(Gd/Yb) _N	1.03	1.15	1.19	1.1	1.22	1.48	1.15	1.23	1.24	1.26	1.15	1.13	1.14	1.04	1.26	1.25
Eu/Eu*	0.36	0.37	0.38	0.76	0.69	0.76	0.59	0.41	0.43	0.58	0.44	0.51	0.42	0.76	0.52	0.82
Sample ID	CH93	CH106		CH123	VM142	VM143	QL167	QL169	QL186	SJ02	SJ04	BA17				
Rock type	GR	QS		GR	QS	GR		GR		GR	GR	GR				
Oxides (wt %)																
SiO ₂	70.41	63.8		67.89	63.97	66.51	68.59	67.42	68.14	66.43	70.56	72.48				
TiO ₂	0.71	1.45		0.68	1.16	1.02	0.33	0.36	0.28	0.85	0.45	0.17				
Al ₂ O ₃	15.96	16.29		15.79	16.65	15.43	16.65	17.05	17.61	16.01	14.51	13.05				
Fe ₂ O ₃	1.25	3.32		1.58	2.19	3.58	2.68	2.85	2.41	4.53	1.27	1.92				
MnO	0.02	0.06		0.03	0.04	0.08	0.07	0.07	0.12	0.07	0.03	0.02				
MgO	0.54	1.26		0.59	1.13	1.58	0.49	0.53	0.35	0.55	0.34	0.13				

(Continued)

Table 4. (Continued)

CaO	2.26	5.13	2.95	5.56	3.81	2.84	2.68	3.03	1.75	1.5	0.59
Na ₂ O	6.65	7.76	6.73	4.43	3.86	5.12	5.36	5.55	5.15	4.65	3.72
K ₂ O	3.21	0.8	0.75	4.72	4.41	3.18	3.09	3.05	5.44	4.48	5.18
P ₂ O ₅	0.11	0.35	0.14	0.31	0.19	0.08	0.08	0.05	0.16	0.06	0.02
LOI	0.39	0.71	1	0.52	0.43	0.8	0.76	0.59	0.81	0.68	0.7
Trace & REEs (ppm)											
V	21	65	38	75	93	27	29	21	62	20	10
Sc	8.6	16.5	9.9	10.7	12.8	1.7	1.9	1.4	8	4.5	3.2
Cr	36	34	36	30	45	48	53	41	36	52	58
Co	1.8	5.9	2.4	3.9	6.1	2.2	2.3	1.9	5.6	3.1	1.6
Ni	2.8	5.2	6.7	4.4	8	3.6	3.6	3.8	7.3	7.1	4
Ga	21.9	23.5	23	22.2	20.7	23.5	22.9	23.8	21	20.3	17.5
Rb	91.5	23.9	24.6	89.4	84.8	88.4	83.5	85	83.8	73.6	143.2
Sr	193.5	208.8	260	297.9	227.2	821.5	822.7	890.5	141.9	192.3	60.8
Y	43.7	46.3	42.1	35.6	28.7	17.9	18.6	17.7	29.6	19.3	31.4
Sn	5	5	5	5	5	5	5	5	5	5	5
Zr	587	455	545	414	616	256	234	264	411	499	260
Nb	28.5	31.6	28.1	24.2	25.5	35.9	37	36.3	23.4	16.4	13.6
Cs	0.49	0.17	0.47	0.45	0.5	1.46	1.55	1.43	0.24	0.23	0.35
Ba	531.8	143	130.8	889.6	822.4	1083.3	1189.2	1277	354.3	273.2	277.4
Hf	12.9	10	12.9	9.7	14.4	6.4	6.4	6.4	10.3	12.9	7
Ta	1.4	1.3	1.3	1.2	1.2	1.4	1.5	1.3	1.2	1.3	1.1
Th	16.64	13.18	10.76	13.59	16.02	10.25	7.11	5.65	16.48	22.18	26.02
U	2.88	3.71	3.07	2.24	3.68	2.7	2.34	1.83	4.25	4.37	4.43
La	30.2	35.8	33.2	25.3	42.6	45.4	45.9	43	18.9	11	34.8
Ce	67.8	82.6	75	53.6	81.4	81.3	84.1	76.5	34.7	20.6	67.3
Pr	8.13	9.93	9.05	6.58	8.48	8.39	8.76	7.85	4.16	2.41	7
Nd	31.6	38.3	33.5	26.8	30	28.6	29.6	26	16.7	9.5	23.6
Sm	6.72	8.19	7.26	6.24	5.45	4.69	5.18	4.34	3.97	2.38	4.67
Eu	1.51	2.13	1.57	2.67	1.4	1.55	1.61	1.48	1.14	1.14	0.32
Gd	6.53	8.22	6.96	5.87	5.04	4.13	4.28	3.61	4.15	2.37	4.48
Tb	1.13	1.32	1.14	0.96	0.77	0.52	0.58	0.48	0.71	0.43	0.75
Dy	7.4	8.29	7.39	6.16	4.61	3.04	3.23	2.81	4.73	2.9	4.92
Ho	1.48	1.65	1.47	1.19	0.95	0.58	0.64	0.55	0.98	0.63	0.99

(Continued)

Table 4. (Continued)

Sample ID	CH93	CH106	CH123	VM142	VM143	QL167	QL169	QL186	SJ02	SJ04	BA17
Rock type	GR	QS	GR	QS	GR	GR	GR	GR	GR	GR	GR
Er	4.85	5.05	4.56	3.68	3.13	1.82	2.02	1.81	3.31	2.25	3.42
Tm	0.7	0.72	0.67	0.53	0.48	0.27	0.28	0.27	0.49	0.35	0.53
Yb	4.74	4.48	4.05	3.24	3.21	1.87	2.03	1.76	3.35	2.32	3.46
Lu	0.8	0.7	0.64	0.51	0.55	0.31	0.33	0.32	0.54	0.41	0.55
ΣREE	173.59	207.38	186.46	143.33	188.07	182.47	188.54	170.78	97.83	58.69	156.79
Ga/Al*10 ⁴	2.59	2.73	2.45	2.52	2.53	2.67	2.54	2.55	2.48	2.64	2.53
Y/Nb	1.53	1.47	1.5	1.47	1.13	0.5	0.5	0.49	1.26	1.18	2.31
A/CNK	0.86	0.71	0.92	0.74	0.85	1	0.98	0.91	0.91	0.95	1.02
(La/Yb) _N	4.34	5.44	5.58	5.31	9.03	16.52	15.39	16.63	3.84	3.23	6.84
(La/Sm) _N	2.82	2.74	2.87	2.54	4.9	6.07	5.55	6.21	2.98	2.9	4.67
(Gd/Yb) _N	1.12	1.49	1.39	1.47	1.27	1.79	1.71	1.66	1	0.83	1.05
Eu/Eu*	0.7	0.79	0.67	1.35	0.82	1.07	1.04	1.14	0.86	1.46	0.21

Note: LOI – loss on ignition; A/CNK = molar Al₂O₃/(CaO + Na₂O + K₂O); N – chondrite normalized; Eu/Eu = Eu_{tot}/(Sm_{tot}Gd_{tot})^{1/2}; wt.% – weight per cent; ppm – part per million; GR – granite; QS – quartz syenite

(25–40 vol. %), which are formed interstitially with K-feldspar and plagioclase. Anhedral to subhedral orthoclase crystals have Carlsbad twinning and are highly perthitic in most samples (Fig. 5a). Subhedral to euhedral plagioclase crystals are less abundant and show polysynthetic twinning (Fig. 5b). Amphibole and biotite (5–10 vol. %) are the main mafic minerals, which are formed along the boundaries of K-feldspar, plagioclase and quartz (Fig. 5a, b). Intergrowth textures (perthitic, granophyric and micrographic) are the main characteristic feature of the granitoids of this group (Fig. 5c). Anti-rapakivi, as an overgrowth texture, is another petrographic feature of the rocks (Fig. 5d). Nevertheless, this feature is not widespread and occurs locally. Deformed fabric such as mylonitic fabric/structure is another common feature of this group, especially in the Galali and Varmaqan granitoid rocks (Fig. 5e) in which the large crystals of K-feldspar, plagioclase and quartz are formed in a fine-grained mass composed of these minerals. Accessory minerals such as zircon, sphene and Fe–Ti oxides are common in these rocks (Fig. 5f).

The second group only includes the Qalaylan massif. The Qalaylan granitoids have a lower K-feldspar content (35–40 vol. %) and relatively higher content (20–35 vol. %) of plagioclase compared to the granitoids of group 1. The rocks have a relatively high quartz content (30–40 vol. %) and amphibole is the dominant mafic mineral, which is formed as euhedral to anhedral crystals (Fig. 5g). In these rocks, dominantly euhedral to subhedral plagioclase crystals are distinctively different from those of group 1. Zoning is the main feature of plagioclase crystals in the Qalaylan granitoids, which is not observed in the massifs of group 1 (Fig. 5h). In some places, zoned plagioclase crystals have been somewhat altered and sericitized in their central parts and have inclusions of accessory minerals, such as sphene and/or zircon (Fig. 5i). Moreover, these granitoids are texturally different in that the K-feldspar crystals are less perthitic and intergrowth textures such as granophyric or micrographic are absent (Fig. 5j).

The third group is actually a subset of group 1 and includes samples from the Galali, Charmaleh and Varmaqan massifs. These rocks show mineralogical and textural features identical to the granitoids of group 1, but in terms of composition, they are relatively different and have much lower amounts of quartz. These rocks have 10–15 vol. % quartz, 70–75 vol. % K-feldspar and 10–20 vol. % plagioclase. K-feldspar crystals are very abundant and in many places perthitic and show Carlsbad twinning (Fig. 5k). The amount of quartz and plagioclase in these rocks is considerably less than other granitoids. Mafic minerals include amphibole and biotite. For the accessory minerals, apatite is more common and has been formed as needle-shaped crystals (Fig. 5l).

The rocks have been given a nomenclature that follows the International Union of Geological Sciences (IUGS) classification. No point counting instrument was used, and, instead, we have used standard graphical charts to estimate the approximate percentage of constituent minerals. In Table 1, the modal values are calculated as a percentage relative to the sum up to 100 %. Finally, on the basis of the approximate percentage of modal minerals (Table 1) the coordinates for a QAP triangle diagram were calculated. Thus, on the basis of the QAP modal classification diagram of Streckeisen (1979), the rocks are mainly granite. As illustrated in the QAP diagram (Fig. 6), the rocks of group 1 are mainly plotted in the syenogranite field and the rocks of the Qalaylan massif (group 2) are much closer to the monzogranite field. Unlike the previous two groups, samples GL21m, CH106 and VM142 as the third group have a lower modal content of quartz (less than 20 %) and, therefore, are placed in the field of quartz syenite.

Table 5. Sr–Nd isotope data for the Almoghlagh–Dehgolan granites

Sample ID	Sr (ppm)	Rb (ppm)	⁸⁷ Rb/ ⁸⁶ Sr	Error (2σ)	⁸⁷ Sr/ ⁸⁶ Sr (Present)	⁸⁷ Sr/ ⁸⁶ Sr (Initial)	Sm (ppm)	Nd (ppm)	¹⁴⁷ Sm/ ¹⁴⁴ Nd	¹⁴³ Nd/ ¹⁴⁴ Nd (Present)	Error (2σ)	¹⁴³ Nd/ ¹⁴⁴ Nd (initial)	eNd (150 Ma)	T _{DM} (Ga)
AM-20m	365	44.0	0.349	0.010	0.707113	0.706382	6.95	29.9	0.141	0.512609	0.00002	0.512471	+0.50	0.95
GL-79	192	6.1	0.092	0.005	0.706071	0.705878	6.34	28.5	0.134	0.512635	0.00002	0.512503	+1.14	0.84
GL-21m	312	105	0.974	0.028	0.707528	0.705486	8.95	39.7	0.136	0.512687	0.00002	0.512553	+2.11	0.76
SH-63	108	154	4.13	0.120	0.712546	0.703887	7.65	38.7	0.120	0.512593	0.00002	0.512475	+0.59	0.78
TK-56	49.1	0.9	0.053	0.005	0.705971	0.705860	8.08	35.5	0.138	0.512693	0.00002	0.512558	+2.20	0.76
TK-82	215	22.0	0.296	0.008	0.706289	0.705668	5.58	27.3	0.124	0.512677	0.00002	0.512555	+2.15	0.68
CH-123	260	24.6	0.274	0.008	0.707119	0.706545	7.26	33.5	0.131	0.512590	0.00002	0.512461	+0.31	0.88
VM-143	227	84.8	1.081	0.031	0.707597	0.705329	5.45	30.0	0.110	0.512552	0.00002	0.512444	-0.02	0.76
QL-169	823	83.5	0.293	0.008	0.704960	0.704344	5.18	29.6	0.106	0.512535	0.00002	0.512431	-0.27	0.76
BA-17	60.8	143	6.81	0.190	0.717059	0.702769	4.67	23.6	0.120	0.512626	0.00002	0.512509	+1.25	0.73

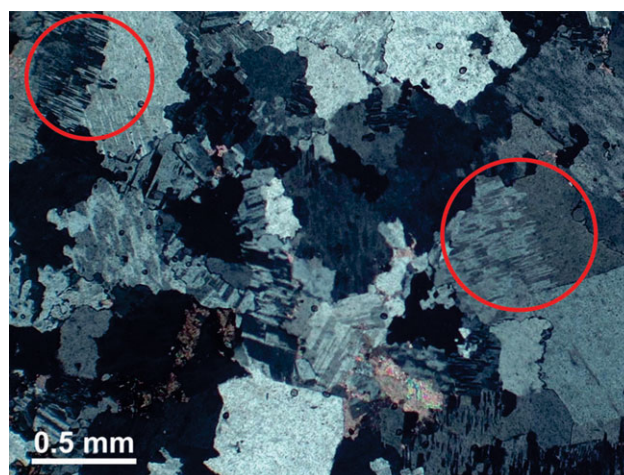


Fig. 7. (Colour online) Photomicrograph showing evidence of replacement of perthitic orthoclase by albite due to Na-metasomatism.

However, Figure 6 shows that the distribution of the samples in the QAP diagram is completely consistent with their petrographic characteristics. In Table 2 the CIPW normative minerals for the samples are presented. The normative values are consistent with the observed petrographic and geochemical features of the samples, because orthoclase crystals are commonly perthitic in these rocks. The amounts of normative anorthite are related to the modal plagioclase, titanite and partly to the amphibole content of the samples. The normative quartz values are consistent with the modal per cent of this mineral.

4. Analytical techniques

Twenty-seven samples from the granitoid bodies were selected for whole-rock chemical analysis. The locations of samples selected for whole-rock analyses are listed in Table 3. Whole-rock chemical analysis was performed at the MSLABS Laboratory in Canada. Major-element oxides were analysed by the inductively coupled plasma emission spectroscopy (ICP-ES) method with a lithium borate fusion. Trace elements and REEs were determined by the inductively coupled plasma mass spectroscopy (ICP-MS) and lithium borate fusion method. The standard samples include STD SY-4 and STD GMN-04. STD OREAS 601 and STD OREAS 24B were used for external calibration. The detection limit was 0.01 wt % for all major-element oxides and less than 0.1 ppm for trace elements. Whole-rock major- and trace-element compositions of the Almoghlagh–Dehgolan granites are listed in Table 4.

Following the petrographic study of 27 thin-sections from the granitic rocks, ten samples were chosen for Nd and Sr isotope analyses at the University of Aveiro (UA), Portugal. For these analyses, the samples were crushed to less than 60 μm. In the Laboratory of Isotope Geology of the UA, the powdered samples were dissolved and submitted to ion chromatography, using the procedures described by Moradi *et al.* (2020). In the same lab, the Sr and Nd isotope ratios were measured using a VG Sector 54 thermal ionization mass spectrometer (TIMS). Mass fractionation was corrected considering ⁸⁸Sr/⁸⁶Sr = 0.1194 and ¹⁴⁶Nd/¹⁴⁴Nd = 0.7219. The analyses using the SRM-987 standard gave an average value of ⁸⁷Sr/⁸⁶Sr = 0.710271 ± 0.000011 (N = 14; confidence limit = 95 %) and the JNdi-1 standard gave an average value of ¹⁴³Nd/¹⁴⁴Nd = 0.5120973 ± 0.0000090 (N = 12;

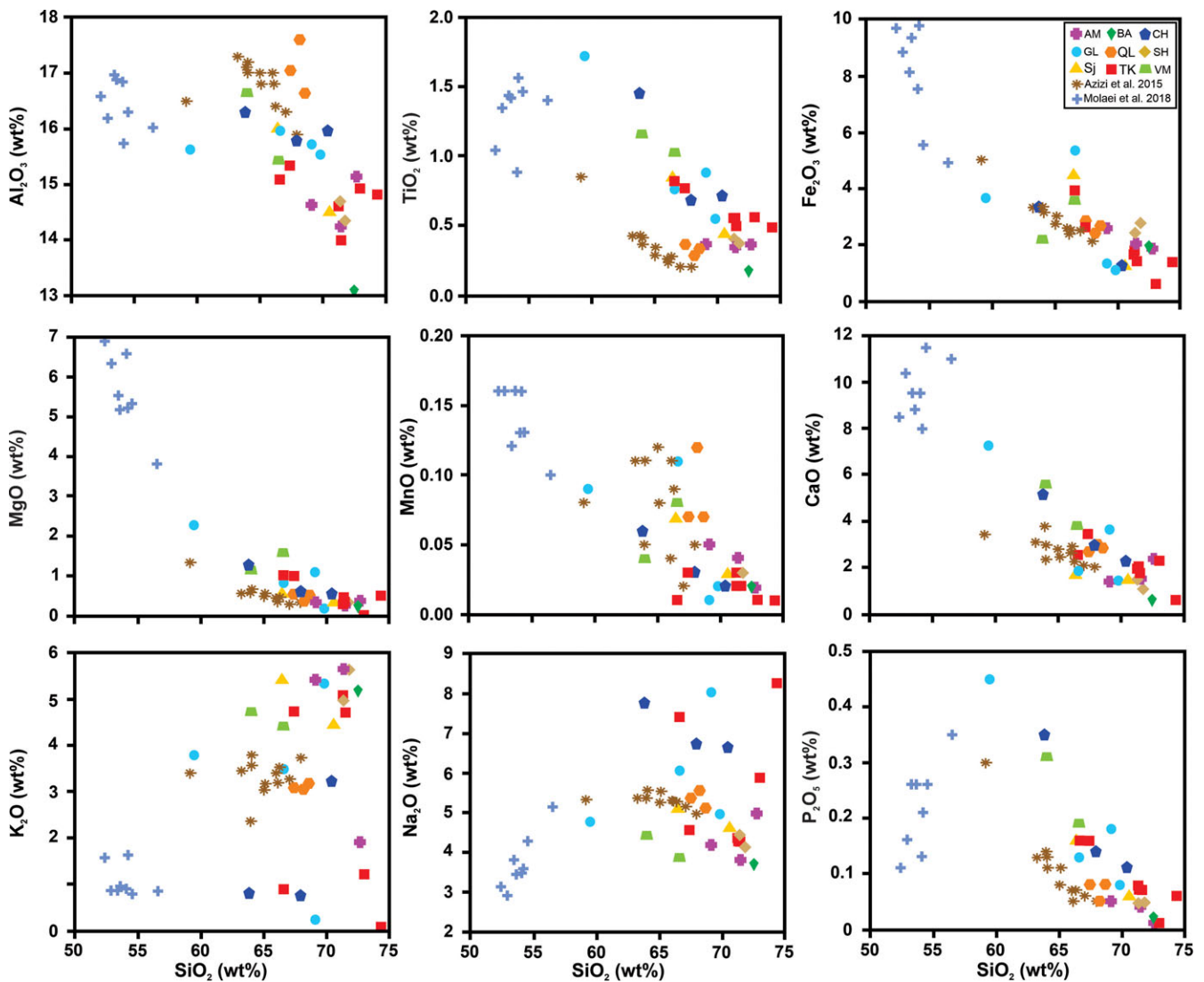


Fig. 8. (Colour online) Harker variation diagrams of major oxides versus SiO_2 for the samples.

confidence limit = 95%). The values of the $^{87}\text{Sr}/^{86}\text{Sr}$ and $^{143}\text{Nd}/^{144}\text{Nd}$ ratios of the studied granites are listed in Table 5.

5. Geochemistry and tectonic setting

5.a. Geochemistry

The granites have SiO_2 values between 59.46 and 74.35 wt % with an average value of 68.99 wt %, except for sample GL21m, which has a lower SiO_2 content (Table 4). The rocks show an average Al_2O_3 content of 15.34 ± 3.31 wt % ($n = 27$) and low TiO_2 , MgO , CaO and P_2O_5 contents. Total alkali contents are high (average = 8.88 ± 0.88 wt %, $n = 27$) and FeO_t content varies between 0.54 and 4.82 wt %. According to the data in Table 4, K_2O shows a relatively wide range of values from 0.06 to 5.64 wt %. Therefore, on the basis of K_2O content, the rocks can generally be categorized into three groups: (1) high-K rocks ($\text{K}_2\text{O} = 4\text{--}6$ wt %), (2) mid-K rocks ($\text{K}_2\text{O} = 2\text{--}4$ wt %) and (3) low-K rocks ($\text{K}_2\text{O} = 0\text{--}2$ wt %).

The group 1, high-K rocks includes samples from the Almoghlagh, Galali, Shirvaneh, Tekyehbala, Varmaqan, Saranjaneh and Bolbanabad massifs. These rocks have high contents of K_2O , which indicates significant amounts of K-bearing

minerals such as K-feldspar (orthoclase). This group can be considered equivalent to the unmetasomatized samples of group 1 of the petrographic classification scheme in which perthitic K-feldspar is the most abundant mineral.

The group 2, mid-K rocks includes mainly the Qalaylan granites and some samples from the Galali and Charmaleh massifs. The rocks of this group have moderate K_2O contents. The Qalaylan granites have the lowest K_2O contents (3.05–3.18 wt %) among the rocks of this group. As discussed in Section 3, plagioclase is the dominant mineral of the granites of the Qalaylan massif, and K-feldspar is less abundant in contrast to the other massifs, which is consistent with their geochemical data. Therefore, the geochemical data for the rocks of this group are in great agreement with their petrographic characteristics and confirm their petrographic classification.

The rocks with low contents of K_2O fall into groups 1 and 3 of Section 3, and they include some samples from the Tekyehbala, Charmaleh, Galali and Almoghlagh massifs. These rocks have K_2O values of between 0.06 and 1.9 wt %. The geochemical data (Table 4) show that the rocks with low K_2O contents have relatively high Na_2O contents. Moreover, the petrographic evidence shows

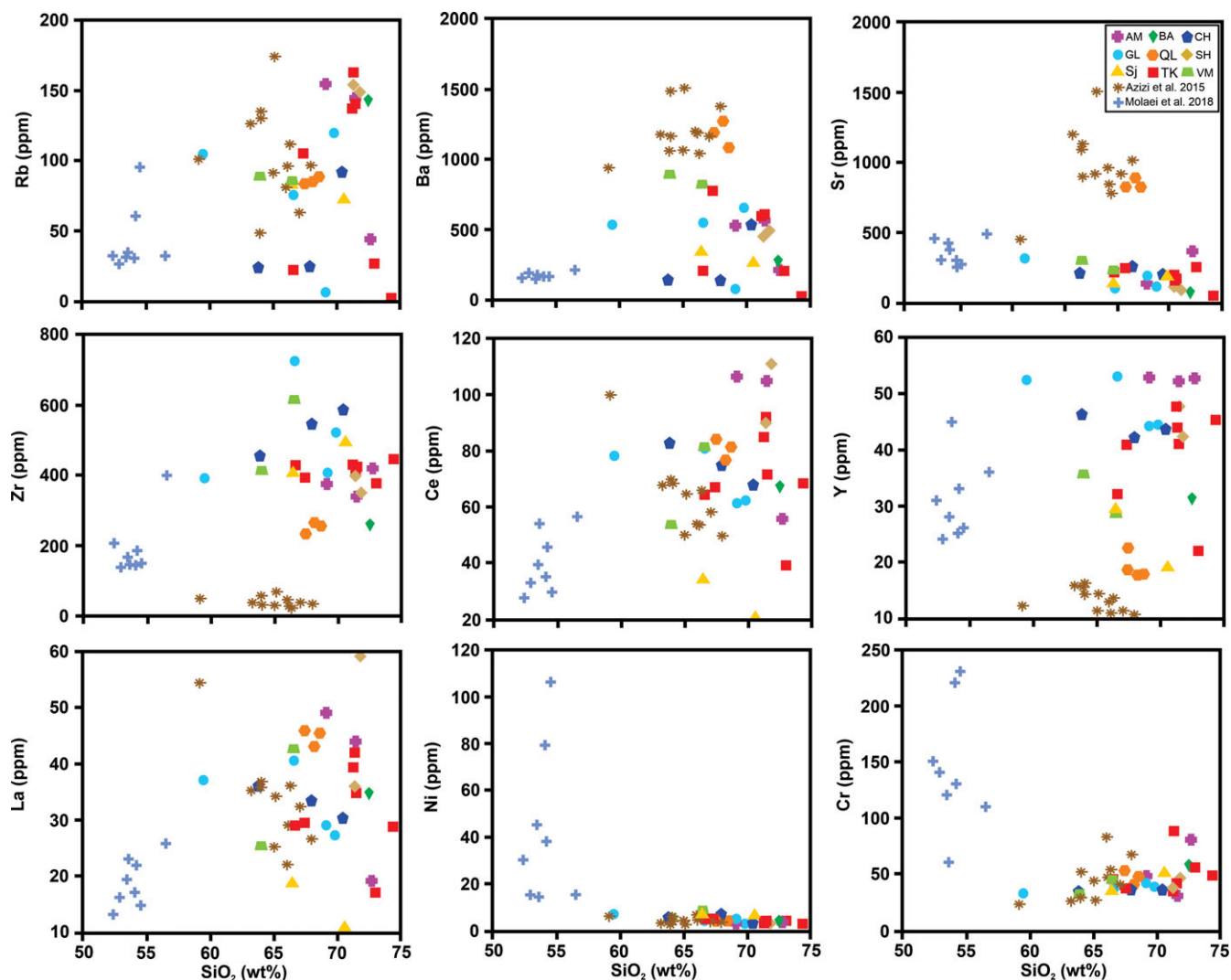


Fig. 9. (Colour online) Harker variation diagrams of trace elements versus SiO_2 for the samples.

that metasomatic processes (i.e. sodic metasomatism) have extensively affected these rocks (Fig. 7). Such a mechanism may cause potassium–sodium exchange between constituent minerals and finally the replacement of K-feldspar (orthoclase) by sodic plagioclase. This feature is obviously seen in the granitoid rocks, especially in the Charmaleh and Tekyehbala massifs. The total amounts of alkali oxides ($\text{K}_2\text{O} + \text{Na}_2\text{O}$) are nearly constant, but the $\text{K}_2\text{O}/\text{Na}_2\text{O}$ ratios are considerably different. Their differences may be due to secondary chemical changes in some samples. The granitoids with various K_2O contents cannot be separated from each other in the field outcrops because no sharp contacts exist between them. On the other hand, replacement textures produced by Na-metasomatism are observable in the thin-sections of low-K samples. Thus, they are not, in fact, separate groups of granitic rocks. As is obvious in the photomicrograph (Fig. 7), albite is not in primary magmatic contact with remnants of orthoclase, and the two minerals have not crystallized simultaneously from the magma. For example, on the right side of Figure 7 and also in the upper left of the figure, albite has no sharp contact with the remnants of orthoclase and albite is gradually replacing orthoclase. If albite had crystallized simultaneously with orthoclase, the whole crystal should show the same relative distribution of albite

throughout the orthoclase and not have one side devoid of any albite. The abundance of the CaO content in such rocks is related to their fairly high titanite content.

Figure 8 shows variation diagrams of major-element oxides versus SiO_2 (Harker, 1909) for the granites. As illustrated in this figure, a negative correlation generally exists between major-element oxides and SiO_2 contents. In most samples, Al_2O_3 , CaO, TiO_2 , MgO, P_2O_5 and Fe_2O_3 contents decrease with increasing SiO_2 amounts. K_2O and Na_2O show relatively scattered trends partly due to secondary alteration and metasomatism. Decreasing trends for major-element oxides indicate their participation in the corresponding minerals. For example, separation of Ca-bearing plagioclases during the early stages of magma generation can reduce the amount of CaO and Al_2O_3 in the melt. Likewise, the trends for TiO_2 , Fe_2O_3 and P_2O_5 can be explained by the presence of accessory minerals, including sphene, Fe–Ti oxides and apatite, which are present in the studied granites.

Multiple plots of trace elements versus SiO_2 for the Almoghlagh–Dehgolan granites are shown in Figure 9. In these diagrams, there is no distinct correlation (negative or positive) between SiO_2 and trace elements. Nevertheless, some trace elements such as Sr and Ba show relatively decreasing trends with

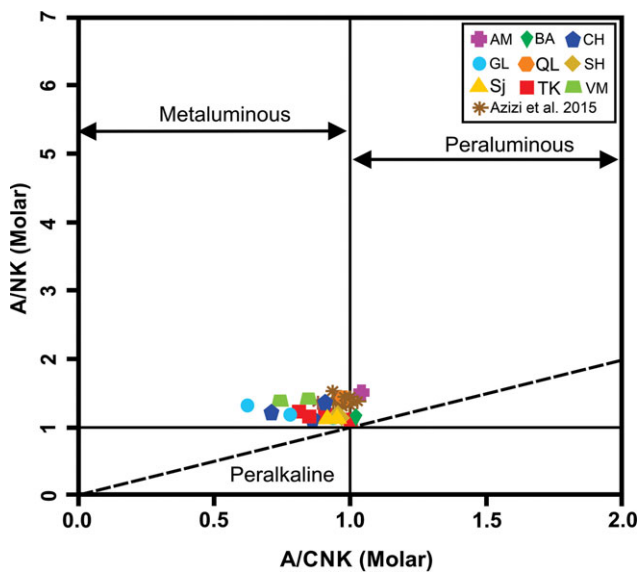


Fig. 10. (Colour online) A/NK versus A/CNK diagram (Shand, 1943) ($A/CNK = \text{molar } Al_2O_3 / (\text{CaO} + \text{Na}_2\text{O} + \text{K}_2\text{O})$ and $A/NK = \text{molar } Al_2O_3 / (\text{Na}_2\text{O} + \text{K}_2\text{O})$). AM – Almoghlagh; GL – Galali; SH – Shirvaneh; TK – Tekyehbala; CH – Charmaleh; VM – Varmaqan; QL – Qalaylan; SJ – Saranjiane; BA – Bolbanabad.

increasing SiO_2 . A decreasing trend for Sr and Ba can be considered in relation to their compatibility in some minerals such as alkali-feldspar and plagioclase, respectively (Rollinson, 1993).

In addition to the Almoghlagh–Dehgolan granites (this study) data for the Qalaylan granitoids (Azizi *et al.* 2015) and gabbroic diorites of the Darvazeh intrusive bodies (Yeganeh *et al.* 2018) are also presented for comparison. As illustrated in Figures 8, 9, the Qalaylan granitoids show trends that are not separate from the studied granites. In contrast, the gabbroic diorites show distinct trends. The different trends for the granites and gabbroic diorites of the area indicate that they most probably are not co-magmatic. Therefore, it can be concluded that these two different rock suites have followed separate magmatic evolution paths and are geochemically independent.

If the $Al_2O_3 / (\text{Na}_2\text{O} + \text{K}_2\text{O})$ versus $Al_2O_3 / (\text{CaO} + \text{Na}_2\text{O} + \text{K}_2\text{O})$ (A/NK versus A/CNK) diagram (Shand, 1943) is used, the studied granites plot mainly in the metaluminous field with $A/CNK = 0.62$ to 1.04 (Fig. 10). Furthermore, in the SiO_2 versus total alkali ($Na_2O + K_2O$) and $(FeO)_t / (FeO_t + MgO)$ diagrams of Frost *et al.* (2001) the samples plot mainly in the alkalic to alkali-calcic and calc-alkalic (Fig. 11a) and ferroan to magnesian fields (Fig. 11b).

The discrimination diagrams of Whalen *et al.* (1987) can be utilized to distinguish the A-type granites from the others. In these diagrams, the Almoghlagh–Dehgolan granites plot mainly in the A-type granite field (Fig. 12). Eby (1992) divided the A-type granites into two groups. As illustrated in Figure 13a, b, with the exception of the Qalaylan granites, all the granites plot in the A_2 -type field. The Yb/Ta versus Y/Nb diagram also shows a similar result for the Qalaylan granites (Fig. 13c). It has been suggested that A_1 -type granitoids have a Y/Nb ratio < 1.2 and that A_2 -types have a Y/Nb ratio > 1.2 (Eby, 1992).

Chondrite-normalized REE patterns (Boynton, 1984) for the Almoghlagh–Dehgolan A-type granites are illustrated in Figure 14. The A-type granites are characterized by enrichment of light rare earth elements (LREEs) relative to heavy rare earth elements (HREEs) with $(La/Yb)_N = 2.44$ – 16.47 . The granites

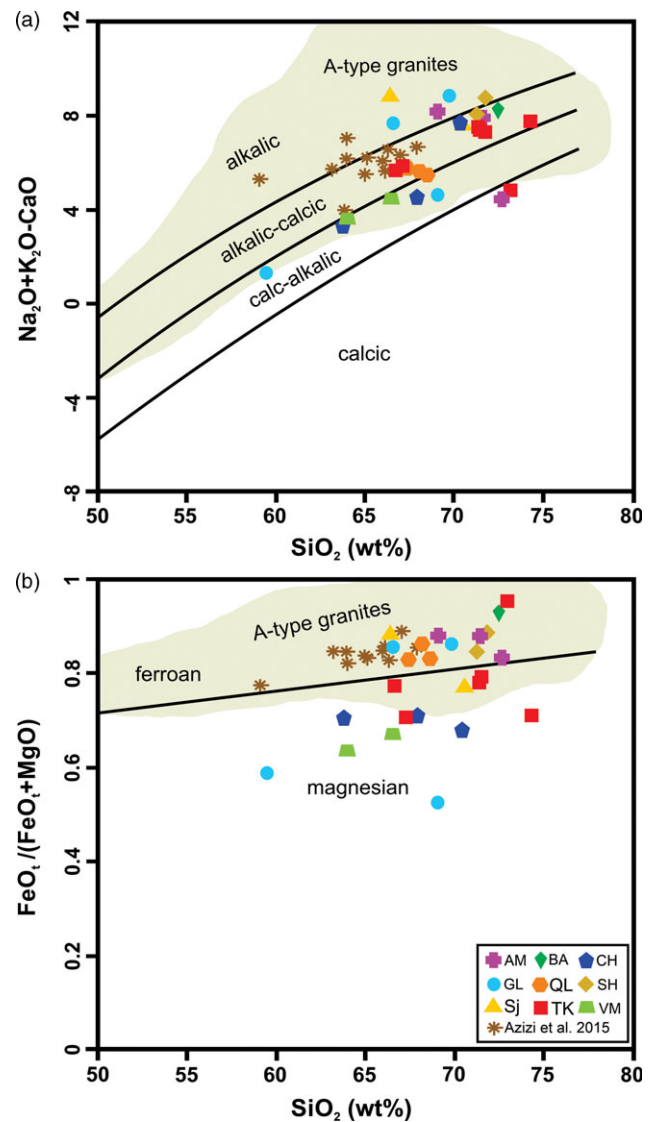


Fig. 11. (Colour online) Geochemical classification diagrams (Frost *et al.* 2001). (a) $Na_2O + K_2O - CaO$ versus SiO_2 diagram. (b) $FeO_t / (FeO_t + MgO)$ versus SiO_2 . AM – Almoghlagh; GL – Galali; SH – Shirvaneh; TK – Tekyehbala; CH – Charmaleh; VM – Varmaqan; QL – Qalaylan; SJ – Saranjiane; BA – Bolbanabad.

display slightly to moderately negative Eu anomalies, whereas some samples have positive anomalies ($Eu/Eu^* = 0.21$ – 1.47 , average value = 0.70). Primitive mantle-normalized trace-element spider diagrams (McDonough & Sun, 1995) show relatively similar characteristics for the Almoghlagh–Dehgolan A-type granites (Fig. 15a). In this diagram, most samples display pronounced negative Nb, P, Ti and Ba anomalies indicative of subduction-related magmatism. They are enriched in Rb, Th and U, and enrichment of Zr is also pronounced in all samples. Lower continental crust-normalized trace-element patterns (Taylor & McLennan, 1995) for the A-type granites of the Almoghlagh–Dehgolan plutons show similarities to the Earth's lower continental crust (Fig. 15b).

5.b. Tectonic setting

The geotectonic discrimination diagrams of Pearce *et al.* (1984) were used to distinguish the tectonic setting of the Almoghlagh–Dehgolan granites (Fig. 16). In these diagrams,

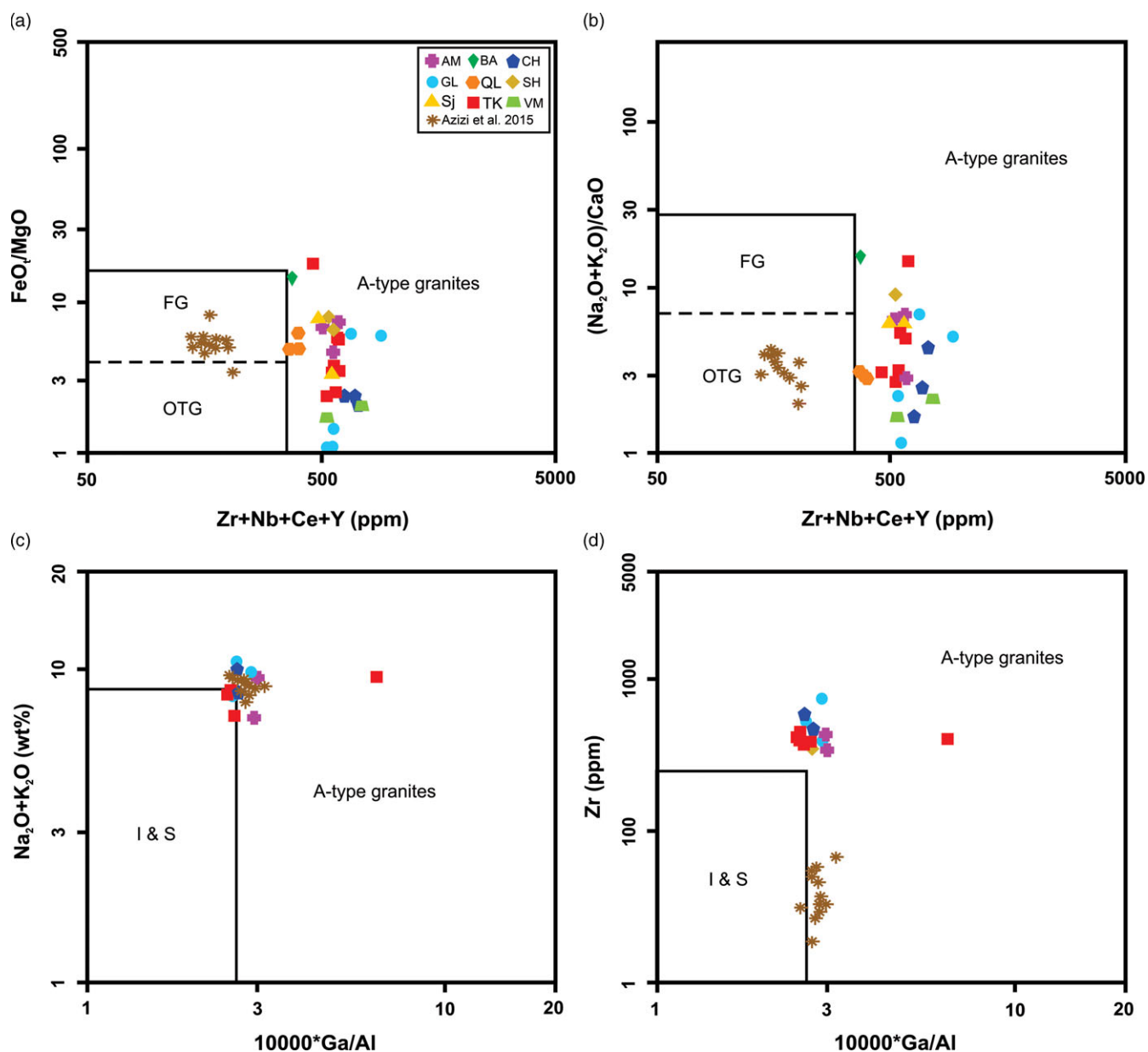


Fig. 12. (Colour online) Geochemical diagrams of Whalen *et al.* (1987) for the discrimination of A-type granites from the other granites. (a) $\text{FeO}_{\text{total}}/\text{MgO}$ versus $\text{Zr} + \text{Nb} + \text{Ce} + \text{Y}$. (b) $(\text{Na}_2\text{O} + \text{K}_2\text{O})/\text{CaO}$ versus $\text{Zr} + \text{Nb} + \text{Ce} + \text{Y}$. (c) $\text{Na}_2\text{O} + \text{K}_2\text{O}$ versus $10\,000 \cdot \text{Ga}/\text{Al}$. (d) Zr versus $10\,000 \cdot \text{Ga}/\text{Al}$. FG – fractionated granites; OTG – other granite types; AM – Almogholagh; GL – Galali; SH – Shirvaneh; TK – Tekyehbala; CH – Charmaleh; VM – Varmaqan; QL – Qalaylan; SJ – Saranjiane; BA – Bolbanabad.

samples plot mainly in the fields of within-plate granites (WPG) and volcanic arc granites (VAG). In the tectonic discrimination diagrams of Schandl & Gorton (2002) the A-type granites plot mainly in the active continental margin (ACM) and within-plate volcanic zone (WPVZ) fields (Fig. 17). In the $3\text{Ta}-\text{Hf}-\text{Rb}/3$ ternary diagram (Harris *et al.* 1986) the samples plot in the volcanic arc (VA) and within-plate (WP) fields (Fig. 18). A common feature of these diagrams is that the Almogholagh–Dehgolan granites plot in the fields of both the volcanic arc and within-plate tectonic settings, which implies a post-orogenic-like tectonic setting.

5.c. Sr–Nd isotopes

Sr–Nd isotopic data for the Almogholagh–Dehgolan granites are presented in Table 5. To calculate the initial Sr and Nd isotope

ratios, the age of 150 Ma was used for the A-type granites, taking into account that this value is within the range of ages reported by Zhang, H. *et al.* (2018). The initial Sr isotope ratios were calculated using the ^{87}Rb decay constant proposed by Villa *et al.* (2015), which is recommended by the IUGS and International Union of Pure and Applied Chemistry (IUAPC). Generally, the Nd isotope compositions result from the magmatic features, and they should not have been significantly affected by post-magmatic processes because both Sm and Nd are relatively mobile elements. In contrast, Rb and Sr are commonly susceptible to modifications during events of hydrothermal and/or meteoric alteration.

For the samples, the initial $^{87}\text{Sr}/^{86}\text{Sr}$ and $^{143}\text{Nd}/^{144}\text{Nd}$ values vary from 0.702769 to 0.706545 and 0.512431 to 0.512558, respectively (Table 5). The Sr–Nd isotope correlation diagram for the Almogholagh–Dehgolan A-type granites is shown in Figure 19.

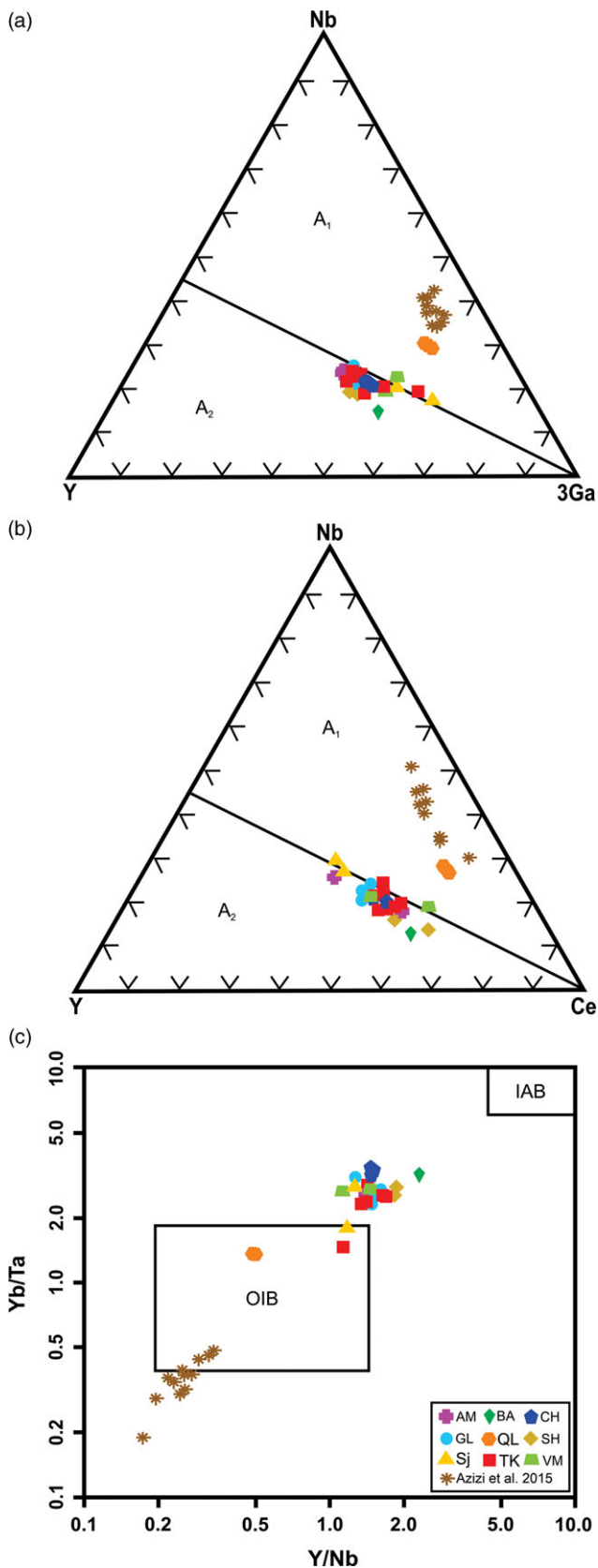


Fig. 13. (Colour online) Geochemical diagrams of Eby (1992) for subdividing A-type granites. (a) Y–Nb–Ga*3. (b) Y–Nb–Ce. (c) Yb/Ta versus Y/Nb. AM – Almoghlagh; GL – Galali; SH – Shirvaneh; TK – Tekyehbala; CH – Charmaleh; VM – Varmaqan; QL – Qalaylan; SJ – Saranjaneh; BA – Bolbanabad; OIB – ocean island basalt; IAB – island arc basalt.

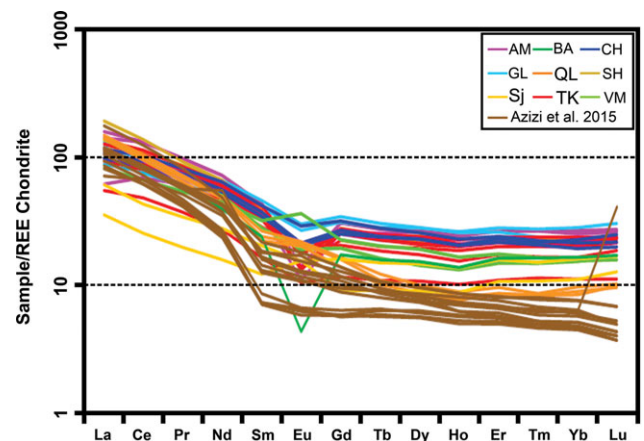


Fig. 14. (Colour online) Chondrite-normalized REE patterns (Boynton, 1984). AM – Almoghlagh; GL – Galali; SH – Shirvaneh; TK – Tekyehbala; CH – Charmaleh; VM – Varmaqan; QL – Qalaylan; SJ – Saranjaneh; BA – Bolbanabad.

For an age of 150 Ma, epsilon Nd (ϵNd) values vary in a relatively limited range, between +2.2 (TK-56) and -0.3 (QL-159). Initial Sr isotope ratios have a significant variation from 0.7028 (BA-17) to 0.7065 (CH-123). The distribution histogram of calculated Nd model ages (T_{DM}) for the Almoghlagh–Dehgolan A-type granites is shown in Figure 20. On the basis of our calculations, the Nd model ages (T_{DM}) range from 0.68 to 0.95 Ga with an average value of 0.79 Ga, which mainly correspond to the Neoproterozoic period.

6. Discussion

Many samples of the Almoghlagh–Dehgolan granites show characteristic features of A-type granites, such as high SiO_2 , FeO/MgO , total alkali (Na_2O , K_2O), Zr, Ga/Al and REEs (except for Eu) and low CaO, MgO and P_2O_5 contents, but samples with lower SiO_2 and lower FeO/MgO ratios also significantly exist. Enriched flat-shaped patterns for HREEs imply that melting of the A-type granite source magma has occurred at pressures lower than the stability field of garnet (Wang *et al.* 2015). Generally, enrichments in large ion lithophile elements and HFSEs are characteristic features of A-type granites (Loiselle & Wones, 1979; Whalen *et al.* 1987; King *et al.* 1997), which are clearly observed in many samples of the Almoghlagh–Dehgolan granites.

As illustrated in Figure 19, the Sr–Nd isotope composition of the Almoghlagh–Dehgolan granites is relatively primitive (similar to the Bulk Silicate Earth). The samples have negative to positive values of $\epsilon\text{Nd}_{(t)}$ and plot in the mantle array with a slight shift to higher $^{87}\text{Sr}/^{86}\text{Sr}_{(t)}$. On the other hand, the existence of inherited zircons (reported by Yajam *et al.* 2015) and elevated Nd model ages (this study) for the studied granites are not consistent with a pure mantle source origin. Nevertheless, it seems that the sources of the parental melts correspond either to mantle and/or crustal rocks. In some places, the granites with mantle-like isotopic ratios could be produced by the reworking of juvenile crustal rocks. As suggested by Dahlquist *et al.* (2010), one of the main sources for the A-type granites is the variable mixture of asthenospheric mantle and continental crust melts. Metaluminous A-type granitic rocks are thought to be derived from a mixture of mantle and crustal components (Schmitt *et al.* 2000; Kemp *et al.* 2005; Bonin, 2007).

We suggest that the derivation of the Almoghlagh–Dehgolan granites from mixed mantle–crustal source materials could well

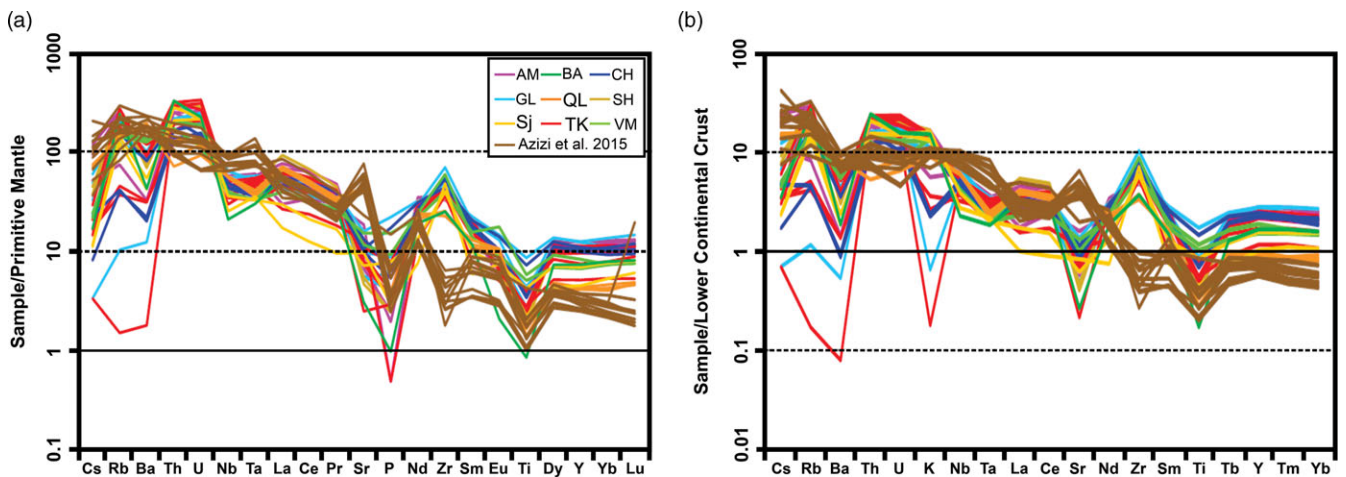


Fig. 15. (Colour online) (a) Primitive mantle-normalized spider diagrams (McDonough & Sun, 1995). (b) Lower continental crust-normalized trace-element patterns (Taylor & McLennan, 1995). AM – Almoghlagh; GL – Galali; SH – Shirvaneh; TK – Tekyehbala; CH – Charmaleh; VM – Varmaqan; QL – Qalaylan; SJ – Saranjaneh; BA – Bolbanabad.

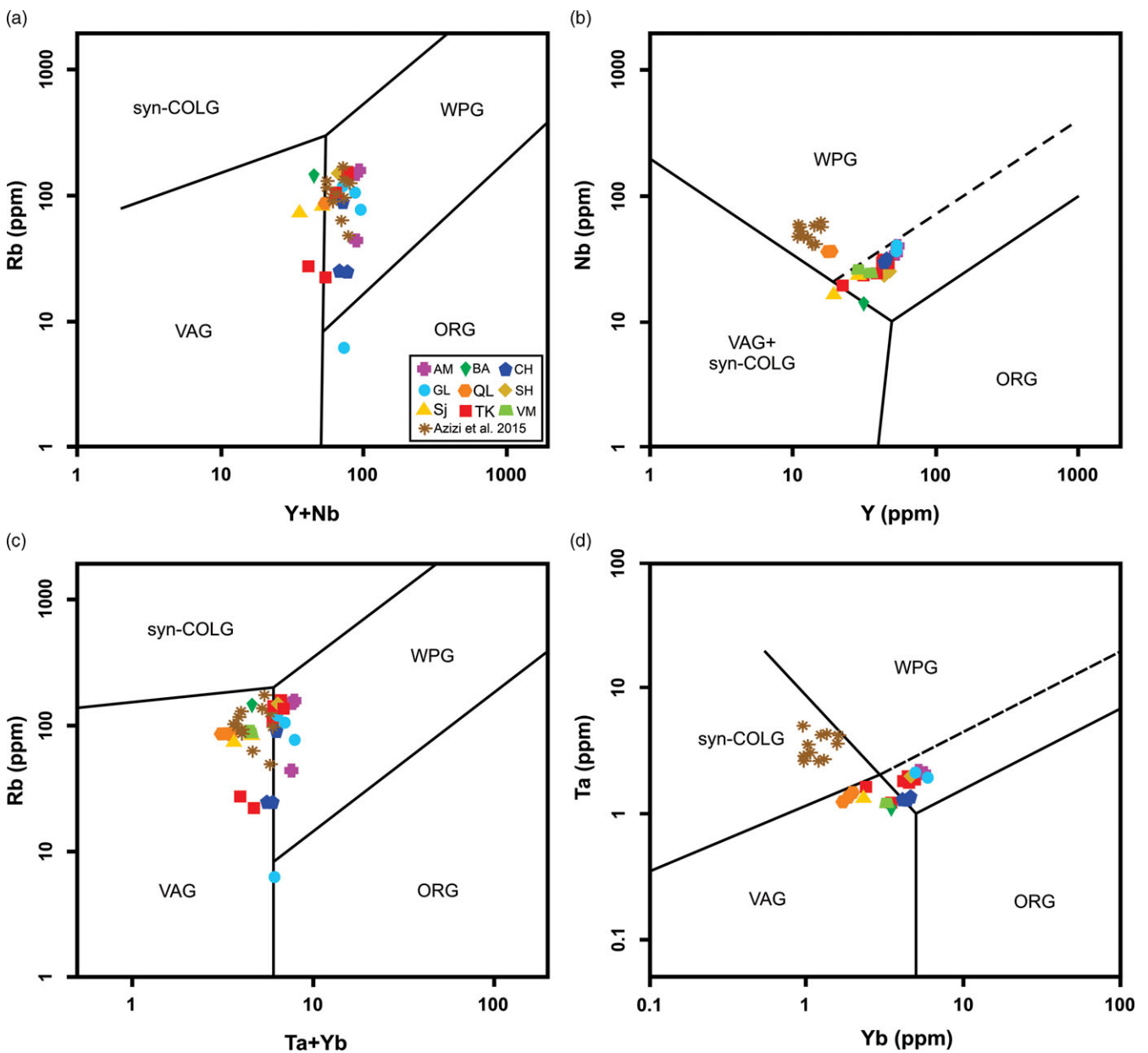


Fig. 16. (Colour online) Geotectonic discrimination diagrams of Pearce *et al.* (1984) for the Almoghlagh–Dehghan A-type granites. (a) Rb versus Y + Nb diagram. (b) Nb versus Y diagram. (c) Rb versus Ta + Yb diagram. (d) Ta versus Yb diagram. Abbreviations: SYN-COLG – syn-collisional granites; WPG – within-plate granites; VAG – volcanic arc granites; ORG – ocean ridge granites; AM – Almoghlagh; GL – Galali; SH – Shirvaneh; TK – Tekyehbala; CH – Charmaleh; VM – Varmaqan; QL – Qalaylan; SJ – Saranjaneh; BA – Bolbanabad.

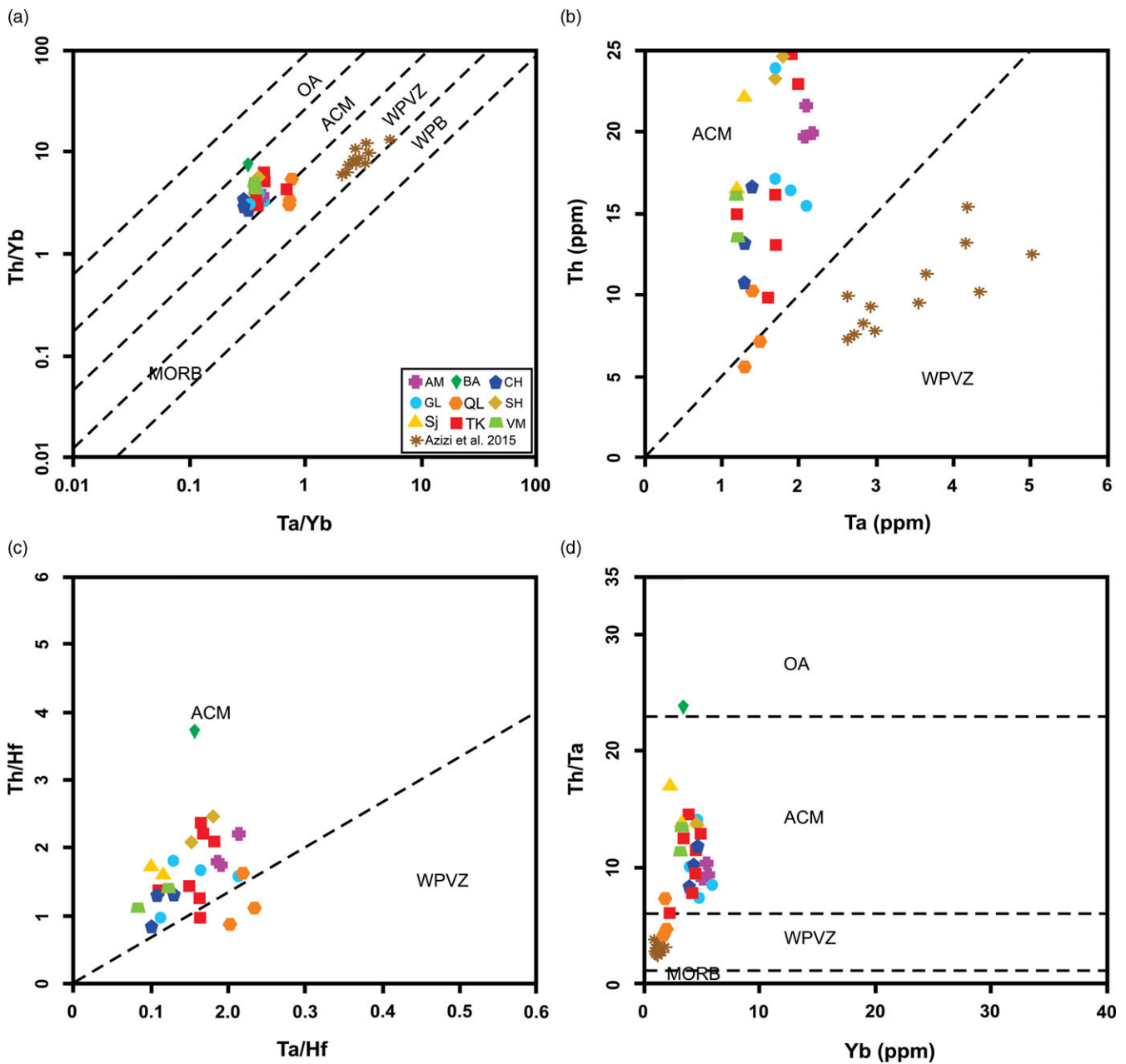


Fig. 17. (Colour online) Geotectonic discrimination diagrams of Schandl & Gorton (2002) for the Almogholagh–Dehghan A-type granites. (a) Th/Yb versus Ta/Yb. (b) Th versus Ta. (c) Th/Hf versus Ta/Hf. (d) Th/Ta versus Yb. Abbreviations: OA – oceanic arcs; ACM – active continental margins; WPVZ – within-plate volcanic zones; WPB – within-plate basalts; MORB – mid-ocean ridge basalts. AM – Almogholagh; GL – Galali; SH – Shirvaneh; TK – Tekyehbala; CH – Charmaleh; VM – Varmaqan; QL – Qalaylan; SJ – Saranjaneh; BA – Bolbanabad.

explain their geochemical and isotopic compositions. The mafic mantle magmas played an important role in providing both the heat and material sources for crustal melting and the generation of the granites.

6.a. Petrogenesis

The rocks mostly show geochemical characteristics of A-type granites (Table 4), and based on the subdivision of Eby (1992) plot in the field of A₂-type granites (with the exception of the Qalaylan granites, which plot in the A₁-type field). Generally, A₂-type granites are related to post-collisional and/or post-orogenic tectonic settings (Eby, 1992). A₂-type granitoids include a greater diversity

of compositions, from metaluminous to peraluminous and peralkaline, and from alkalic to calc-alkalic (Frost & Frost, 2011). These granitoids have mixed geochemical signatures of continental crust and island arc (Wu *et al.* 2002). Placement of the Almogholagh–Dehghan granites in the post-orogenic setting field can also be explained by an extensional tectonic setting in the subduction environment of the SaSZ.

On the basis of the transitional nature of the Almogholagh–Dehghan granites, their formation by fractionation of I-type melts is unlikely. Many investigators (e.g. Maanijou *et al.* 2013; Sarjoughian *et al.* 2015; Yajam *et al.* 2015; Amiri *et al.* 2017; Jamshidibadr *et al.* 2018) have studied the mafic rocks of the Qorveh region and adjacent areas in the NSaSZ. On the basis of

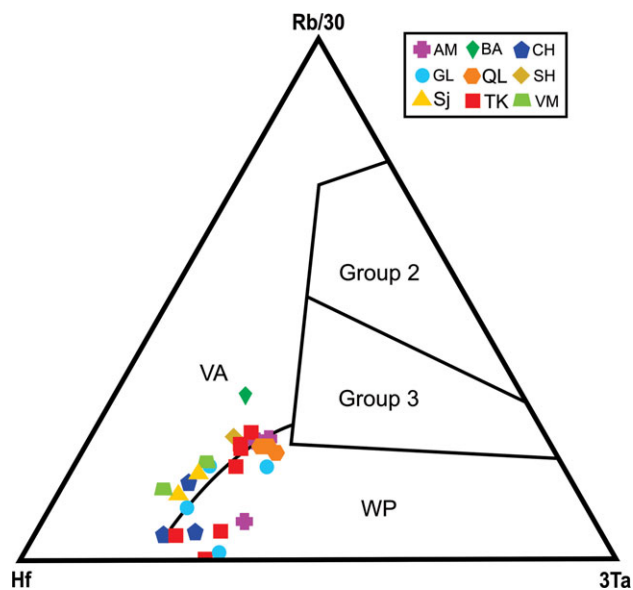


Fig. 18. (Colour online) 3Ta–Hf–Rb/30 tectonic discrimination diagram (Harris *et al.* 1986). Abbreviations: VA – volcanic arcs; WP – within-plate; Group 2 – syn-collision; Group 3 – late-post collision. AM – Almoghlagh; GL – Galali; SH – Shirvaneh; TK – Tekyehbala; CH – Charmaleh; VM – Varmaqan; QL – Qalaylan; SJ – Saranjaneh; BA – Bolbanabad.

their investigations, these rocks have the geochemical characteristics of arc-type magmas and are related to subduction of the Neo-Tethys oceanic crust. The mafic rocks mainly have a mantle source, and there is no genetic relationship between these rocks with the granitic rocks of the region.

Fractionation of alkaline basaltic magmas causes the formation of alkaline granites, which is in contrast with the metaluminous nature of the granites of the Almoghlagh–Dehgolan. Owing to the lack of field evidence of magma mixing (such as mafic enclaves) in the Almoghlagh–Dehgolan granites, the role of mixing processes in their formation is not clear. However, in some parts of the region coeval intrusion of mafic and felsic rocks probably indicates magma mingling processes. Magma evolution diagrams (Fig. 21a, b) show that the Almoghlagh–Dehgolan granites follow the trend of partial melting rather than fractional crystallization, which implies that the partial melting process (regardless of the source type) had an important role in the generation of the granite magma source.

The granites have little or no depletion in HREEs, which rules out garnet as an important phase during their petrogenesis. On the other hand, the granites of the Almoghlagh–Dehgolan cannot be formed by the partial melting of metasedimentary components, because, in this case, the resultant granites are mainly peraluminous whereas the Almoghlagh–Dehgolan granites are metaluminous. Relatively high contents of K_2O and Na_2O in the Almoghlagh–Dehgolan granites indicate the existence of plagioclase and K-feldspar or biotite in their source. In addition, negative Sr anomalies accompanied by high HREE contents indicate the presence of plagioclase and the absence of garnet in their source (Watkins *et al.* 2007).

One of the basic requirements for the generation of A-type granites by partial melting of crustal materials is an external heat source. Mantle-derived mafic magmas could supply heat and fluid to facilitate the partial melting of crustal rocks (Gao *et al.* 2016). The Qalaylan granites show different geochemical features relative

to the other granites. These granites have geochemical characteristics of calc-alkaline I-type granites. Moreover, the lack of intergrowth textures such as perthitic texture in these rocks is one of the main petrographic differences with A-type granites. On the basis of petrographic, geochemical and geochronological (older age) characteristics of the Qalaylan granites in comparison to the other A₂-type granites in the Almoghlagh–Dehgolan region, their formation mechanism may be different. We suggest that the Qalaylan I-type granites were formed during the earlier stages (159 ± 3 Ma; Yajam *et al.* 2015) of the Neo-Tethys subduction, and their apparent pseudo-A₁ affinity has been acquired by metasomatic fluids, which makes them similar to those of ocean island basalt (OIB)-like magma sources. On the basis of the geochemical and isotopic compositions, the formation of the metaluminous A₂-type granites of the Almoghlagh–Dehgolan is most likely related to partial melting of lower crustal dry rocks with a considerable contribution of mafic magmas from the mantle.

6.b. Geodynamic notes

Generally, geochemical differences between I- and A-type granites indicate their different tectonic environments. Yan & Shi (2016) suggested that I-type granites are related to compression and the A-type ones are related to extension. Therefore, co-development of roughly contemporaneous I- and A-type granites in the NSaSZ (Almoghlagh–Dehgolan region) indicates the geodynamic changes under which these two different types of granites were formed.

The Almoghlagh–Dehgolan granites (this study) share transitional geochemical characteristics of I- to A-type granites with more A-type affinities. In geotectonic discrimination diagrams, the rocks mainly plot in the fields of volcanic arc and within-plate granites. These granites may correspond to a shift from pure I-type to pure A-type granites and, therefore, from collisional to post-orogenic stages of the SaSZ orogenic belt during Jurassic time. But, considering the geological history of the SaSZ (i.e. the lack of continent–continent collision during Jurassic time) this issue cannot be well explained by a simple ocean–continent subduction model. Therefore, considering the field, petrographic and geochemical characteristics of the granites (this study) and the geodynamic constraints of the NSaSZ during Jurassic time, we may compare two possible weakly extensional geodynamic models (an intra-arc extensional tectonic setting and a post-arc–continent collision environment) for the generation of the granites, but each model should be considered with some uncertainties. As previously mentioned by some authors (e.g. Sarjoughian *et al.* 2015), too, there is a transitional I-type to A-type magmatism in the region that possibly resulted from no pure and pervasive extensional regime at the time and a local transition from a compressional to weakly extensional period.

During Early–Late Jurassic time, arc magmas were generated owing to subduction of the Neo-Tethys oceanic crust beneath the Central Iranian Microplate. Mantle-derived mafic magmas have geochemical characteristics typical of volcanic arc magmas related to an active continental margin setting. Underplating of these mafic magmas into the lower crust has caused melting or/and modification of the crustal rocks. Geochemically, Early–Middle Jurassic granitoids of the SaSZ are I-type. These I-type granites are mainly calc-alkaline and plot in the VAG field of tectonic discrimination diagrams (e.g. Ahmadi Khalaji *et al.* 2007; Mahmoudi *et al.* 2011; Esna-Ashari *et al.* 2012; Maanijou *et al.* 2013; Sepahi *et al.* 2018; Tavakoli *et al.* 2021). Moreover, different

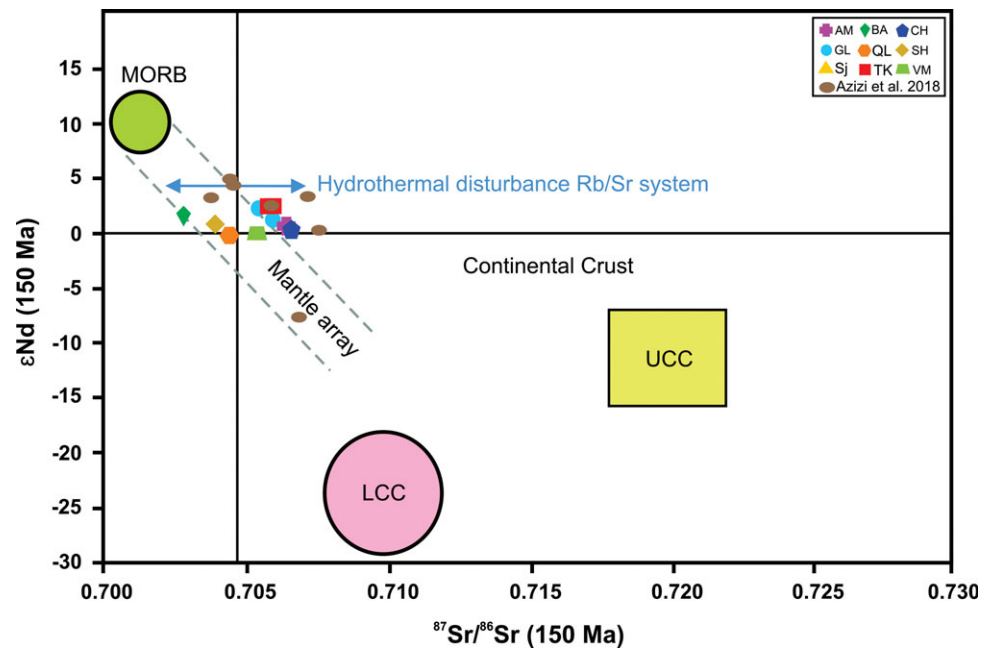


Fig. 19. (Colour online) ϵNd versus $^{87}\text{Sr}/^{86}\text{Sr}$ correlation diagram (modified after Zindler & Hart, 1986). UCC – upper continental crust; LCC – lower continental crust; AM – Almogholagh; GL – Galali; SH – Shirvaneh; TK – Tekyehbala; CH – Charmaleh; VM – Varmaqaan; QL – Qalaylan; SJ – Saranjaneh; BA – Bolbanabad.

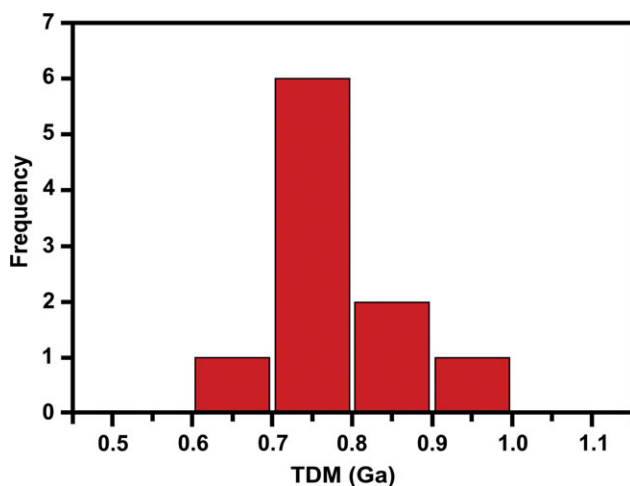


Fig. 20. (Colour online) Histogram of Nd model age frequency for the Almogholagh-Dehgolan A-type granites.

sources from mantle to crustal materials have been suggested for their generation.

Subsequent Late Jurassic magmatism may have been triggered in a continental extensional environment, probably a back-arc tectonic setting (Moinevaziri *et al.* 2015; Zhang, Z. *et al.* 2018). However, there are serious objections to the extensional back-arc model (i.e. due to the slab roll-back mechanism) at 150 Ma in the region. On the other hand, transition from a compressional to an extensional geodynamic model has been previously suggested for the region (Sarjoughian *et al.* 2015; Yajam *et al.* 2015). Considering all available evidence, we suggest that a local intra-arc extensional environment may explain the formation of A-type granites in the region. In this model, as the subduction continued, deep strike-slip faults caused the development of a local extensional environment. These extensional structures facilitated the ascent and emplacement of asthenospheric magmas into the lower

crust. Subsequently, mantle convection caused the asthenosphere to upwell. Mantle-derived magmas played an important role in the generation of A-type granites by providing heat and source materials. As discussed earlier, Sr–Nd isotopic data show a mixed mantle–crustal source for the Almogholagh–Dehgolan granites. Finally, we suggest that partial melting of dry lower crustal rocks (i.e. a charnockite-like lithology) with a contribution of mantle mafic magmas was the main mechanism for the generation of A-type granites in the region.

The third alternative model could be a late-orogenic model (a stage between the collision to post-orogenic stage), but arguing about the possible existence of many models will just complicate the geodynamic interpretation of the region. Therefore, we prefer not to propose another new model for the region.

As has been explained in Section 1, different controversial models have been proposed for the geodynamic evolution of the SaSZ. However, the majority are concentrated on a continental magmatic arc setting as a part of an orogenic belt. Finding an exclusive model consistent with all available geological data that occur in the SaSZ is truly difficult. For example, recently Azizi & Stern (2019) presented a propagating rift model to interpret Jurassic magmatism in the region, but on the basis of huge volumes of calc-alkaline plutonic rocks, this model may not be a model that correlates with geological observations. We agree with most other authors such as Torkian *et al.* (2008), Shahbazi *et al.* (2010), Agard *et al.* (2011), Sepahi *et al.* (2013, 2018) and Hassanzadeh & Wernicke (2016), who have argued for a subduction-related environment (continental arc or active continental margin) for a petrogenetic interpretation of the region in Jurassic time.

The Zagros orogeny is intimately linked with the closure of the Neo-Tethys (from subduction to collision). Subduction of the Neo-Tethys below Eurasia probably happened from Late Triassic or Early Jurassic time onwards, as testified by arc magmatism in the SaSZ (Agard *et al.* 2011). The latter authors also argued that collision and progressive build-up of the Zagros orogen took place from Oligocene time ($\sim 30 \pm 5$ Ma). Their investigations show that continent–continent collision did not happen during Jurassic time.

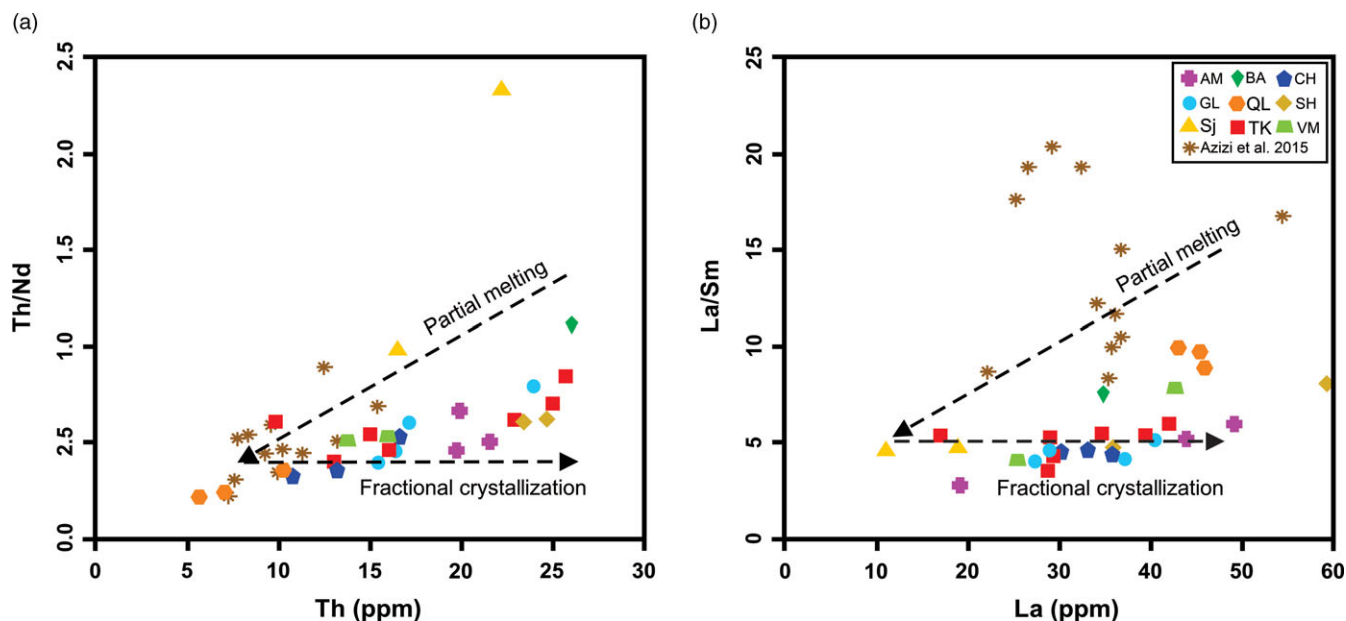


Fig. 21. (Colour online) Magma evolution diagrams for the Almogholagh–Dehgolan A-type granites. (a) Th/Nd versus Th diagram. (b) La/Sm versus La diagram. The trends of partial melting and fractional crystallization are modified after Kong *et al.* (2018). AM – Almogholagh; GL – Galali; SH – Shirvaneh; TK – Tekyehbala; CH – Charmaleh; VM – Varmaqaan; QL – Qalaylan; SJ – Saranjianeh; BA – Bolbanabad.

7. Conclusions

Our new geochemical data indicate that most of the Almogholagh–Dehgolan granites share characteristic features of A-type granites. With the exception of the Qalaylan granites, all the granites are A_2 -type. On the basis of geotectonic discrimination diagrams, these metaluminous A_2 -type granites were formed in a subduction-related extensional tectonic setting. The Qalaylan granites have geochemical features of I-type granites and are not A-type. The results of the Sr–Nd isotope analysis show that, for an age of 150 Ma, the initial $^{87}\text{Sr}/^{86}\text{Sr}$ ratios vary in a wide range. Contrary to the Sr isotope ratios, ϵNd values vary in a limited range. Calculated Nd model ages (T_{DM}) mainly correspond to the Neoproterozoic period. However, Sr–Nd isotope characteristics of the Almogholagh–Dehgolan granites are relatively primitive (similar to the Bulk Earth). Nd isotopic data indicate mixed mantle–crustal materials acted as the source for the A-type granites. We suggest a geodynamic model involving partial melting of lower crustal rocks for the generation of the A-type granites. In this model, contemporaneous mantle-derived mafic magmas played an important role as the heat sources for partial melting of the lower crustal rocks and/or as part of magmas responsible for the generation of the A-type granites. This process has occurred in a weakly extensional environment. I-type granites of the SaSZ are representatives of compression episodes, whereas A-type granites are representatives of extension episodes. Therefore, the co-development of these two types of granites in the region indicates transitional geodynamic changes from compressional to extensional during Late Jurassic time in the NSaSZ.

Acknowledgements. This work was financially supported by the Iran National Science Foundation (INSF), [grant number: 96013382-2017] as a part of Ph.D. thesis at Bu-Ali Sina University, Hamedan, Iran. The authors also gratefully acknowledge Professor Lorence G. Collins for his constructive comments on editing of the manuscript.

Conflict of interests. None.

References

- Agard P, Omrani J, Jolivet L, Whitechurch H, Vrielynck B, Spakman W, Monie P, Meyer B and Wortel R (2011) Zagros orogeny: a subduction-dominated process. *Geological Magazine* **148**, 692–725.
- Ahmadi Khalaji A, Esmaeily D, Valizadeh MV and Rahimpour-Bonab H (2007) Petrology and geochemistry of the granitoid complex of Boroujerd, Sanandaj–Sirjan Zone, Western Iran. *Journal of Asian Earth Sciences* **29**, 859–77.
- Alirezaei S and Hassanzadeh J (2012) Geochemistry and zircon geochronology of the Permian A-type Hasanrobat granite, Sanandaj–Sirjan belt: a new record of the Gondwana break-up in Iran. *Lithos* **151**, 122–34.
- Amiri M, Ahmadi Khalaji A, Tahmasbi Z, Santos JF, Zarei Sahahmieh R and Zamanian H (2017) Geochemistry, petrogenesis, and tectonic setting of the Almogholagh batholith in the Sanandaj–Sirjan zone, western Iran. *Journal of African Earth Sciences* **134**, 113–33.
- Arvin M, Pan Y, Dargahi S, Malekizadeh A and Babaei A (2007) Petrochemistry of the Siah-Kuh granitoid stock southwest of Kerman Iran: implications for initiation of Neotethys subduction. *Journal of Asian Earth Sciences* **30**, 474–89.
- Azizi H (2020) Reply to comment on “Jurassic igneous rocks of the central Sanandaj–Sirjan zone (Iran) mark a propagating continental rift, not a magmatic arc” by Azizi and Stern (Terra Nova 31, 415–423, 2019). *Terra Nova* **32**, 473–75.
- Azizi H and Asahara Y (2013) Juvenile granite in the Sanandaj–Sirjan Zone, NW Iran: Late Jurassic–Early Cretaceous arc–continent collision. *International Geology Review* **55**, 1523–40.
- Azizi H, Asahara Y, Minami M and Anma R (2020) Sequential magma injection with a wide range of mixing and mingling in Late Jurassic plutons, southern Ghorveh, western Iran. *Journal of Asian Earth Sciences* **200**, 104469. doi: 10.1016/j.jseas.2020.104469.
- Azizi H, Mohammadi K, Asahara Y, Tsuboi M, Daneshvar N and Mehrabi B (2016) Strongly peraluminous leucogranite (Ebrahim-Attar granite) as evidence for extensional tectonic regime in the Cretaceous, Sanandaj–Sirjan zone, Northwest Iran. *Geochemistry* **76**, 529–41.
- Azizi H, Nouri F, Stern RJ, Azizi M, Lucci F, Asahara Y, Zarinkoub MH and Chung SL (2018) New evidence for Jurassic continental rifting in the northern Sanandaj Sirjan Zone, western Iran: the Ghalaylan seamount, southwest Ghorveh. *International Geology Review* **62**, 1635–57.

- Azizi H and Stern RJ** (2019) Jurassic igneous rocks of the central Sanandaj–Sirjan zone (Iran) mark a propagating continental rift, not a magmatic arc. *Terra Nova* **31**, 415–23.
- Azizi H, Zanjefili-Beiranvand M and Asahara Y** (2015) Zircon U–Pb ages and petrogenesis of a tonalite–trondhjemite–granodiorite (TTG) complex in the northern Sanandaj–Sirjan zone, northwest Iran: evidence for Late Jurassic arc–continent collision. *Lithos* **216**, 178–95.
- Balen D, Schneider P, Massone HJ, Opitz J, Luptáková J, Putiš M and Petrinc Z** (2020) The Late Cretaceous A-type alkali-feldspar granite from the Mt. Požeška (N. Croatia): potential marker of fast magma ascent in the Europe–Adria suture zone. *Geologica Carpathica* **71**, 361–81.
- Bonin B** (2007) A-type granites and related rocks: evolution of a concept, problems and prospects. *Lithos* **97**, 1–29.
- Bonin B, Janoušek V and Moyen JF** (2020) Chemical variation, modal composition and classification of granitoids. In *Post-Archean Granitic Rocks: Contrasting Petrogenetic Processes and Tectonic Environments* (eds V Janoušek, B Bonin, WJ Collins, F Farina and B Bowden), pp. 9–51. Geological Society of London, Special Publication no. 491.
- Boynton WV** (1984) Geochemistry of the rare earth element: meteorite studies. In *Rare Earth Element Geochemistry* (ed. P Henderson), pp. 89–92. Amsterdam: Elsevier.
- Collins WJ, Beams SD, White AJR and Chappell BW** (1982) Nature and origin of A-type granites with particular reference to southeastern Australia. *Contributions to Mineralogy and Petrology* **80**, 189–200.
- Cowgill E, Forte AM, Niemi N, Avdeev B, Tye A, Trexler C, Javakhishvili Z, Elashvili M and Godoladze T** (2016) Relict basin closure and crustal shortening budgets during continental collision: an example from Caucasus sediment provenance. *Tectonics* **35**, 2918–47.
- Dahlquist JA, Alasino PH, Eby GN, Galindo C and Casquet C** (2010) Fault controlled Carboniferous A-type magmatism in the proto-Andean foreland (Sierras Pampeanas, Argentina): geochemical constraints and petrogenesis. *Lithos* **115**, 65–81.
- Eby GN** (1990) The A-type granitoids: a review of their occurrence and chemical characteristics and speculations on their petrogenesis. *Lithos* **26**, 115–34.
- Eby GN** (1992) Chemical subdivision of the A-type granitoids; petrogenetic and tectonic implications. *Geology* **20**, 641–4.
- Eby GN** (2011) A-type granites: magma sources and their contribution to the growth of the continental crust. In *Abstracts, Seventh Hutton Symposium on Granites and Related Rocks, Avila, Spain, 4–9 July 2011*, pp. 50–1.
- Elahi-Janatmakan F, Maghdour-Mashhour R and Tabakh Shabani AA** (2020) Comment on “Jurassic igneous rocks of the central Sanandaj–Sirjan zone (Iran) mark a propagating continental rift, not a magmatic arc” by Azizi and Stern (Terra Nova 31, 415–423, 2019). *Terra Nova* **32**, 468–72.
- Eshraghi SA, Jafarian MB and Eghlimi B** (1996) *1:100000 Geological Map of Qorveh*. Tehran: Geological Survey of Iran.
- Eshraghi SA and Mahmoudi Gharai M** (2003) *1:100000 Geological Map of Tuyserkhan*. Tehran: Geological Survey of Iran.
- Eсна-Ashari A, Tiepolo M, Valizadeh MV, Hassanzadeh J and Sepahi AA** (2012) Geochemistry and zircon U–Pb geochronology of Aligoodarz granitoid complex, Sanandaj–Sirjan Zone, Iran. *Journal of Asian Earth Sciences* **43**, 11–22.
- Fazlnia A, Schenk V, Van Der Straaten F and Mirmohammadi M** (2009) Petrology, geochemistry and geochronology of trondhjemites from the Qori complex, Neyriz, Iran. *Lithos* **112**, 413–33.
- Frost BR, Barnes CG, Collins WJ, Arculus RJ, Ellis DJ and Frost CD** (2001) A geochemical classification for granitic rocks. *Journal of Petrology* **42**, 2033–48.
- Frost CD and Frost BR** (2011) On ferroan (A-type) granitoids: their compositional variability and modes of origin. *Journal of Petrology* **52**, 39–53.
- Gao P, Zheng YF and Zhao ZF** (2016) Experimental melts from crustal rocks: a lithochemical constraint on granite petrogenesis. *Lithos* **266**, 133–57.
- Grebennikov AV** (2014) A-type granites and related rocks: petrogenesis and classification. *Russian Geology and Geophysics* **55**, 1074–86.
- Harker A** (1909) *The Natural History of Igneous Rocks*. New York: Macmillan, 384 pp.
- Harris NBW, Pearce JA and Tindle AG** (1986) Geochemical characteristics of collision-zone magmatism. In *Collision Tectonics* (eds MP Coward and AC Ries), pp. 67–81. Geological Society of London, Special Publication no. 19.
- Hassanzadeh J and Wernicke BP** (2016) The Neotethyan Sanandaj–Sirjan zone of Iran as an archetype for passive margin–arc transitions. *Tectonics* **35**, 586–621.
- Hosseini M, Mosawery F and Karimynia M** (1999) *1:100000 Geological Map of Qorveh*. Tehran: Geological Survey of Iran
- Hunziker D, Burg JP, Bouilhol P and von Quadt A** (2015) Jurassic rifting at the Eurasian Tethys margin: geochemical and geochronological constraints from granitoids of North Makran, southeastern Iran. *Tectonics* **34**, 571–93.
- Jamshidibadr M, Collins AS, Salomao GN and Costa M** (2018) U–Pb zircon ages, geochemistry and tectonic setting of felsic and mafic intrusive rocks of Almoghlagh complex, NW Iran. *Periodico di Mineralogia* **87**, 21–53.
- Kemp AIS, Wormald RJ, Whitehouse MJ and Price RC** (2005) Hf isotopes in zircon reveal contrasting sources and crystallization histories for alkaline to peralkaline granites of Temora, southeastern Australia. *Geology* **33**, 797–800.
- King PL, White AJR, Chappell BW and Allen CM** (1997) Characterization and origin of aluminous A-type granites from the Lachlan Fold Belt, Southeastern Australia. *Journal of Petrology* **38**, 371–91.
- Kong H, Li H, Wu QH, Xi XS, Dick JM and Gabo-Ratio JAS** (2018) Co-development of Jurassic I-type and A-type granites in southern Hunan, South China: dual control by plate subduction and intraplate mantle upwelling. *Geochemistry* **78**, 500–20.
- Lechmann A, Burg JP, Ulmer P, Mohammadi A, Guillong M and Faridi M** (2018) From Jurassic rifting to Cretaceous subduction in NW Iranian Azerbaijan: geochronological and geochemical signals from granitoids. *Contributions to Mineralogy and Petrology* **173**, 1–16.
- Loiselle MC and Wones DR** (1979) Characteristics and origin of anorogenic granites. *Geological Society of America Abstracts with Programs* **11**, 468.
- Lu J, Zhang C and Liu D** (2020) Geochronological, geochemical and Sr–Nd–Hf isotopic studies of the A-type granites and adakitic granodiorites in Western Junggar: petrogenesis and tectonic implications. *Minerals* **10**, 397. doi: [10.3390/min10050397](https://doi.org/10.3390/min10050397).
- Maanijou M, Aliani F, Miri M and Lentz DR** (2013) Geochemistry and petrology of igneous assemblage of Qorveh area, west Iran. *Geochemistry* **73**, 181–96.
- Maghdour-Mashhour R, Hayes B, Pang KN, Bolhar R, Tabakh Shabani AA and Elahi-Janatmakan F** (2021) Episodic subduction initiation triggered Jurassic magmatism in the Sanandaj–Sirjan zone, Iran. *Lithos* **396**, 106189. doi: [10.1016/j.lithos.2021.106189](https://doi.org/10.1016/j.lithos.2021.106189).
- Mahmoudi S, Corfu F, Masoudi F, Mehrabi B and Mohajjel M** (2011) U–Pb dating and emplacement history of granitoid plutons in the northern Sanandaj–Sirjan Zone, Iran. *Journal of Asian Earth Sciences* **41**, 238–49.
- Mansouri Esfahani M, Khalili M, Kochhar N and Gupta LN** (2010) A-type granite of the Hasanrobat area (NW of Isfahan, Iran) and its tectonic significance. *Journal of Asian Earth Sciences* **37**, 207–18.
- McDonough WF and Sun SS** (1995) The composition of the Earth. *Chemical Geology* **120**, 223–53.
- McQuarrie N, Stock JM, Verdel C and Wernicke BP** (2003) Cenozoic evolution of Neo-Tethys and implications for the causes of plate motions. *Geophysical Research Letters* **30**, 2036. doi: [10.1029/2003GL017992](https://doi.org/10.1029/2003GL017992).
- Mehdipour Ghazi J and Moazzen M** (2015) Geodynamic evolution of the Sanandaj–Sirjan Zone, Zagros Orogen, Iran. *Turkish Journal of Earth Sciences* **24**, 513–28.
- Mohajjel M and Fergusson CL** (2000) Dextral transpression in Late Cretaceous continental collision, Sanandaj–Sirjan zone, western Iran. *Journal of Structural Geology* **22**, 1125–39.
- Moinevaziri H, Akbarpour A and Azizi H** (2015) Mesozoic magmatism in the northwestern Sanandaj–Sirjan zone as an evidence for active continental margin. *Arabian Journal of Geosciences* **8**, 3077–88.
- Molaei T, Torkian A, Christiansen EH and Sepahi AA** (2018) Petrogenesis of the Darvazeh mafic–intermediate intrusive bodies, Qorveh, Sanandaj–Sirjan, Iran. *Arabian Journal of Geosciences* **11**, 1–20.
- Monfaredi B, Hauzenberger C, Neubauer F, Schulz B, Shakerardakani F, Genser J and Halama R** (2016) Reconstruction of the metamorphic evolution of the Hamadan high-grade metapelites, Sanandaj–Sirjan Zone, western

- Iran. In *European Geoscience Union General Assembly 2016, Vienna, Austria, 17–22 April 2016. Geophysical Research Abstracts* **18**, EGU2016-13377.
- Moradi A, Shabanian N, Davoudian AR, Azizi H, Santos JF and Asahara Y** (2020) Geochronology and petrogenesis of the Late Neoproterozoic granitic gneisses of Golpayegan Metamorphic Complex: a new respect for Cadomian crust in the Sanandaj-Sirjan Zone, Iran. *International Geology Review* **64**, 1450–73.
- Omrani J, Agard P, Whitechurch H, Benoit M, Prouteau G and Jolivet L** (2008) Arc-magmatism and subduction history beneath the Zagros Mountains, Iran: a new report of adakites and geodynamic consequences. *Lithos* **108**, 380–98.
- Pearce JA, Harris NBW and Tindle AG** (1984) Trace element discrimination diagrams for granitic rocks. *Journal of Petrology* **25**, 956–83.
- Richards JP, Spell T, Rameh E, Raziq A and Fletcher T** (2012) High Sr/Y magmas reflect arc maturity, high magmatic water content, and porphyry Cu \pm Mo \pm Au potential: examples from the Tethyan arcs of central and eastern Iran and western Pakistan. *Economic Geology* **107**, 295–332.
- Rollinson HR** (1993) *Using Geochemical Data: Evaluation, Presentation, Interpretation*. London: Longman Science & Technical, 384 pp.
- Sarjoughian F, Kananian A, Hashchke M and Ahmadian J** (2015) Transition from I-type to A-type magmatism in the Sanandaj-Sirjan zone, NW Iran: an extensional intra-continental arc. *Geological Journal* **51**, 387–404.
- Schandl ES and Gorton MP** (2002) Application of high field strength elements to discriminate tectonic settings in VMS environments. *Economic Geology* **97**, 629–42.
- Schmitt AK, Emmermann R, Trumbull RB, Buhn B and Henjes-Kunst F** (2000) Petrogenesis and $^{40}\text{Ar}/^{39}\text{Ar}$ geochronology of the Brandberg Complex, Namibia: evidence for a major mantle contribution in metaluminous and peralkaline granites. *Journal of Petrology* **41**, 1207–39.
- Sepahi AA and Athari SF** (2006) Petrology of major granitic plutons of the northwestern part of Sanandaj-Sirjan metamorphic belt, Zagros Orogen, Iran: with emphasis on A-type granitoids from SE Saqqez area. *Neues Jahrbuch für Mineralogie-Abhandlungen: Journal of Mineralogy and Geochemistry* **183**, 93–106.
- Sepahi AA, Borzoei K and Salami S** (2013) Mineral chemistry and thermobarometry of plutonic, metamorphic and anatectic rocks from the Tueyserkan area (Hamedan, Iran). *Geological Quarterly* **57**, 515–26.
- Sepahi AA, Salami S, Lentz D, McFarlane C and Maanijou M** (2018) Petrography, geochemistry, and U–Pb geochronology of pegmatites and aplites associated with the Alvand intrusive complex in the Hamedan region, Sanandaj–Sirjan zone, Zagros orogen (Iran). *International Journal of Earth Sciences* **107**, 1059–96.
- Shafaii Moghadam H, Li QL, Li XH, Stern RJ, Levresse G, Santos JF, Lopez Martinez M, Ducea MN, Ghorbani G and Hassannezhad A** (2020) Neotethyan subduction ignited the Iran arc and back arc differently. *Journal of Geophysical Research: Solid Earth* **125**, e2019JB018460. doi: [10.1029/2019JB018460](https://doi.org/10.1029/2019JB018460).
- Shahbazi H, Siebel M, Ghorbani M, Pourmoafi M, Sepahi AA, VosoughiAbedini M and Shang CK** (2015) The Almoghlagh pluton, Sanandaj-Sirjan zone, Iran: geochemistry, U–(Th)-Pb titanite geochronology and implications for its tectonic evolution. *Neues Jahrbuch für Mineralogie-Abhandlungen: Journal of Mineralogy and Geochemistry* **192**, 85–99.
- Shahbazi H, Siebel W, Pourmoafie M, Ghorbani M, Sepahi AA, Shang CK and Vosoughi-Abedini M** (2010) Geochemistry and U–Pb zircon geochronology of the Alvand plutonic complex in Sanandaj–Sirjan zone (Iran): new evidence for Jurassic magmatism. *Journal of Asian Earth Sciences* **39**, 668–83.
- Shakerardakani F, Li XH, Neubauer F, Ling XX, Li J, Monfaredi B and Wu LG** (2020) Genesis of early cretaceous leucogranites in the Central Sanandaj-Sirjan zone, Iran: reworking of Neoproterozoic metasedimentary rocks in an active continental margin. *Lithos* **352**, 105330. doi: [10.1016/j.lithos.2019.105330](https://doi.org/10.1016/j.lithos.2019.105330).
- Shand SJ** (1943) *The Eruptive Rocks Their Genesis, Composition, Classification and Their Relation to Ore Deposits*. New York: Wiley, 444 pp.
- Shellnutt JG and Zhou MF** (2007) Permian peralkaline, peraluminous and metaluminous A-type granites in the Panxi district, SW China: their relationship to the Emeishan mantle plume. *Chemical Geology* **243**, 286–316.
- Streckeisen A** (1979) Classification and nomenclature of volcanic rocks, lamprophyres, carbonatites and millitic rocks: recommendations and suggestions of IUGS sub-commission on the systematics of igneous rocks. *Geology* **7**, 331–5.
- Tavakoli N, Shabanian N, Davoudian AR, Azizi H, Neubauer F, Asahara Y, Bernroider M and Lee JKW** (2021) A-type granite in the Boein-Miandasht Complex: evidence for a Late Jurassic extensional regime in the Sanandaj-Sirjan Zone, western Iran. *Journal of Asian Earth Sciences*, **213**, 104771. doi: [10.1016/j.jseaes.2021.104771](https://doi.org/10.1016/j.jseaes.2021.104771).
- Taylor SR and McLennan SM** (1995) The geochemical evolution of the continental crust. *Reviews of Geophysics* **33**, 241–65.
- Torkian A, Khalili M and Sepahi AA** (2008) Petrology and geochemistry of the I-type calc-alkaline Qorveh Granitoid Complex, Sanandaj-Sirjan Zone, western Iran. *Neues Jahrbuch für Mineralogie-Abhandlungen: Journal of Mineralogy and Geochemistry* **185**, 131–42.
- Verdel C, Wernicke BP, Hassanzadeh J and Guest B** (2011) A Paleogene extensional arc flare-up in Iran. *Tectonics* **30**, TC3008. doi: [10.1029/2010TC002809](https://doi.org/10.1029/2010TC002809).
- Villa IM, De Bièvre P, Holden NE and Renne PR** (2015) IUPAC-IUGS recommendation on the half life of ^{87}Rb . *Geochimica et Cosmochimica Acta* **164**, 382–5.
- Wang GC, Jiang YH, Liu Z, Ni CY, Qing L and Zhang Q** (2015) Elemental and Sr–Nd–Hf isotopic constraints on the origin of Late Jurassic adakitic granodiorite in central Fujian province, southeast China. *Mineralogy and Petrology* **109**, 501–18.
- Watkins J, Clemens J and Treloar P** (2007) Archaean TTGs as sources of younger granitic magmas: melting of sodic metatonalites at 0.6–1.2 GPa. *Contributions to Mineralogy and Petrology* **154**, 91–110.
- Whalen JB, Currie KL and Chappell BW** (1987) A-type granites: geochemical characteristics, discrimination and petrogenesis. *Contributions to Mineralogy and Petrology* **95**, 407–19.
- Whalen JB and Hildebrand RS** (2019) Trace element discrimination of arc, slab failure, and A-type granitic rocks. *Lithos* **348**, 105179. doi: [10.1016/j.lithos.2019.105179](https://doi.org/10.1016/j.lithos.2019.105179).
- Whitney DL and Evans BW** (2010) Abbreviations for names of rock-forming minerals. *American Mineralogist* **95**, 185–7.
- Wu FY, Sun DY, Li H, Jahn BM and Wilde S** (2002) A-type granites in northeastern China: age and geochemical constraints on their petrogenesis. *Chemical Geology* **187**, 14–173.
- Yajam S, Montra P, Scarrow J, Ghalamghash J, Razavi SMH and Bea F** (2015) The spatial and compositional evolution of the Late Jurassic Qorveh-Dehghan plutons of the Zagros Orogen, Iran: SHRIMP zircon U–Pb and Sr and Nd isotope evidence. *Geologica Acta: An International Earth Science Journal* **13**, 25–43.
- Yan QS and Shi XF** (2016) Geochronology of the Laoshan granitic complex in eastern China and its tectonic implications. *Geological Journal* **51**, 137–48.
- Yang TN, Chen JL, Liang MJ, Xin D, Aghazadeh M, Hou ZQ and Zhang HR** (2018) Two plutonic complexes of the Sanandaj–Sirjan magmatic-metamorphic belt record Jurassic to Early Cretaceous subduction of an old Neo-Tethys beneath the Iran microplate. *Gondwana Research* **62**, 246–68.
- Yeganeh TM, Torkian A, Christiansen EH and Sepahi AA** (2018) Petrogenesis of the Darvazeh mafic-intermediate intrusive bodies, Qorveh, Sanandaj-Sirjan, Iran. *Arabian Journal of Geosciences* **11**, 1–20.
- Zahedi M and Hajian J** (1985) *1:250000 Geological Map of Sanandaj*. Tehran: Geological Survey of Iran.
- Zhang H, Chen J, Yang T, Hou Z and Aghazadeh M** (2018) Jurassic granitoids in the northwestern Sanandaj–Sirjan zone: evolving magmatism in response to the development of a Neo-Tethyan slab window. *Gondwana Research* **62**, 269–86.
- Zhang Z, Xiao WX, Ji W, Majidifard MR, Rezaeian M, Talebian M, Xiang D, Chen L, Wan B, Ao S and Esmaili R** (2018) Geochemistry, zircon U–Pb and Hf isotope for granitoids, NW Sanandaj-Sirjan zone, Iran: implications for Mesozoic–Cenozoic episodic magmatism during Neo-Tethyan lithospheric subduction. *Gondwana Research* **62**, 227–45.
- Zindler A and Hart S** (1986) Chemical geodynamics. *Annual Review of Earth and Planetary Sciences* **14**, 493–571.